AERODESIGN SOLUTIONS

PRIVATE LIMITED

www.aerodesignsolutions.com

CONVENTIONAL AIRCRAFT WING BOX PRELIMINARY DESIGN

Submitted by -
Date:
Place:

Signature:
Name:

Submitted to -
Date:
Place:

Signature:
Name:

AERODESIGN SOLUTIONS PRIVATE LIMITED
#69, 1st Floor, 5th Cross, Ramanjaneya Layout,
Marathahalli, Bangalore, Karnataka, India, 560037
CIN: U74999KA2016PTC092492

DECLARATION

Date: 06/08/2018 Title of the Project: CONVENTIONAL AIRCRAFT WING BOX PREMILINARY DESIGN

I understand that Aerodesign Solution Private Limited shall hold the copyrights of all project/dissertations submitted to it.

I will republish the entire report / extracts of the project only with the permission of Aerodesign Solution Private Limited and I am liable to pay 40% of royalty to the Company.

If I engage in documenting any research findings with an intention of publishing it for commercial purpose, I shall obtain a NOC from the Director prior to engaging in such activities.

Name of the candidate: Ezeorah Godswill Uchechukwu

Signature of the candidate:

APPROVAL/CERTIFICATE

ACKNOWLEDGEMENT

I give all praise and glory to the LORD GOD Almighty for his mighty presence throughout the research work to finish it successfully.

I would like to thank the founders of Aerodesign Solutions Private Limited Mr. Satish Hiremath and Mr. Pawan Rama Mali for extending this wonderful opportunity. they were my supervisors, I am so thankful for all their patience in helping me out with the new concept with teaching and guidance, which are so valuable for me to gain an expertise in this Air-foil analysis. I am so honoured to have worked with them, to learn and experience their expertise in the field of Aircraft design. I am grateful to them for being there whenever I needed their advice.

I would also like to thank staff Mr. Chandan NS, for his support and motivation.

At last, it would be impossible without the wholehearted support of my family and friends, they believed in me to undertake a unique, phenomenal and outstanding project, in which they continuously provided an unwinding support, that helped me a lot in the successful completion of this research.

ABSTRACT

The plain Wing Box of a two-seater conventional aircraft is modelled with the help of Catia. This is exported to other software/tools, in order to be subjected to analysis of its torsional strength, stress/bending moment distribution, shear, etc. on the component parts of the wing box. The type of wing selected with its component parts are described in details, in regards to its individual contribution and necessity to the overall wing box structural strength and manufacturability. For the case of simplified study, the first wing has been chosen to have a circulation cross section for the stringers (skin stiffeners), two trans-versing spar (span wise) and several axially (with reference to the fuselage axis) placed webbed rib between the spars. Also describing the basic structure of a wing and the components used in it. The function of stringers and spars, the longitudinal stiffeners in the wing. The designing of spars in a wing is also shown with the help of screenshots in CATIA V5 software. Load representative of an aircraft will be considered in this study. The wing-box model is further analysed with Ansys software for structural optimization (i.e. Mass, stress, twist etc.), through the consideration of different parameters.

TABLE OF CONTENTS

LIST OF FIGURES

LIST OF TABLES

1 INTRODUCTION

The three most important, structured components of an aircraft, namely the wings, fuselage and empennage, are considered from the point of view of stressing as beams or cantilevers with variable loading along their lengths. Aircraft wing consists of basic components like stringers running along the wing spar, ribs positioned at different stations along spanwise direction, front and rear spars; upper and lower skins as shown in fig. 1. Each of these components act like a beam and torsion member as a whole. The wing-box is built in the assembly jigs where all the ribs and spars are loaded in a specific sequence. This is given in five stages:

1) Complete structure assembly, i.e. ribs, front spar, rear spar.
2) Slaved and drilling of top skin panel.
3) Slaved and drilling of bottom skin panel.
4) Installation of bottom skin panel.
5) Installation of top skin panel.

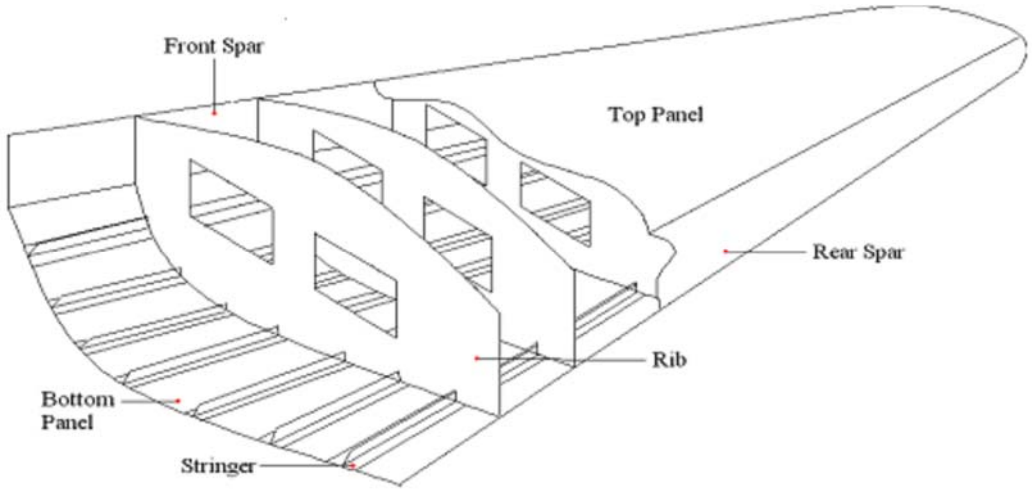

Figure 1 Wing box components

Assembly of the wing box is a very time consuming and labor-intensive process using manual drilling and fastening methods with dedicated jigs and fixtures. Preferably, much of this process should be carried out automatically. Removal of the misalignments

occurring during part-to-part assembly is however a necessary pre-automation challenge. Recent studies conducted in Airbus UK highlights dimensional problems within aircraft structure during the assembly process. It has been observed that a completed wing that has come out of the assembly jig was twisted due to change in the structural shape during assembly. This could be attributed to the rib profile that may have changed during installation of the panels. This emphasizes a serious difference between the expected profile and the profile obtained during and after the assembly process.

1.1 PURPOSE

The wing box structure will be designed and analysed for a two-seater conventional aircraft

1.2 REQUIREMENTS FOR ITS GIVEN MISSION PROFILE

Range : 926km = 3040000ft
Vcruise : 66.88m/s = 219, 44ft/s
hcruise : 2440m = 8000ft
Wcrew : 100kg = 220, 26lb
Wpayload : 100kg = 220, 26lb

The below results and data were obtained from Principles of Aircraft Design Project Report (on Conceptual Design of a Two Seat General Aviation Aircraft):

The takeoff mass (W0), empty mass (We) and fuel mass (Wf) of the designed aircraft are estimated from the calculations as follows:

W0 = 2041,88lb = 926.18119 kg
We = 1222,19lb
Wf = 216, 988lb = 98, 5kg

Thrust to mass ratio and wing loading

Wing loading can also be calculated as the ratio of maximum takeoff mass to wing wetted area.

Swet(wing) = 19.82m^2

Wing loading (Wtakeoff/Swet(wing)) = 2041,88/213.3407 = 9.571 Ib/ft^2

Hence we can say that a safty factor of about 1.776 was consider to take the wing loading as 17 Ib/ft^2

Horsepower To Mass Ratio $(hp/W)_{takeoff}$	0, 085
Wing Loading $(W/S)_{takeoff}$	17 lb/ft^2
C_{lmax} (Plain Flaps)	1,8
V_{stall} (sea level, standard day, landing conf.)	52,77 knots
V_{stall} (sea level, standard day, takeoff conf.)	59 knots
V_{stall} (sea level, standard day, cruise)	55,95 knots
V_{stall} (5000ft, hot day, landing conf.)	59,22 knots
Take off Ground Roll (sea level, standard day)	1000ft(304, 8)
Take off field length (seal level, standard day)	1300ft(396, 24m)
Landing Ground Roll (seal level ,standard day)	755,56ft(230,3m)
Landing Field Length (seal level ,standard day)	1355,56ft(413,18m)
Altitude (for best range)	24447, 43ft(7451, 6m)
$M_{best\ range}$ (sea level)	0, 214
(L/D)max	13, 52
hpcruise/hptakeoff	0,415
Vbest endurance (loiter) (sea level)	61, 5 knots

Instantaneous Turn Rate (cruising altitude)	34,658 deg/s
Climb Gradient (G) (Beginning of Climb)	0, 2332
Rate of climb (Vy) (Beginning of Climb)	27, 87 ft/s
Climb Gradient (G) (End of Climb)	0,0835
Rate of climb (Vy) (End of Climb)	18, 65 ft/s
Maximum Ceiling	39128, 5ft(11926, 4m)

Characteristics of wing

Characteristics	WING
Airfoil	NACA 4415
Aspect Ratio	7
Wing Sweep(l.e.)	8,6°
Wing Sweep(c/4)	4°
Taper ratio (λ)	0,4
Twist	untwist
Dihedral	0°
Incidence	2°
Wing Tip	Sharp
Wing Vertical Location	Mid

Aerodynamic properties

Results are tabulated below:

		Clean at M = 0.2	**Takeoff Flapped at M = 0.2**	***Landing Flapped at M = 0.2***
CL - α	**$C_{l\alpha}$ (1/deg)**	0,0929	0,11	0,11
	C_{Lmax}	1,526	1,761	1,862
	$\alpha_{L=0}$ (deg)	-1,2	-5,35	-7,42
	α_{Clmax} (deg)	14,67	12,66	11,51
	$\Delta\alpha_{Clmax}$ (deg)	2	2	2

Table 10.3 *Lift calculations*

		Clean at M = 0.2	***Takeoff Flapped at M = 0.2***	***Landing Flapped at M = 0.2***

C_L - C_D	**C_D**	$0{,}038+0{,}0542C_L^2$	$0{,}0656+0{,}0542C_L^2$	$0{,}0932+0{,}0542C_L^2$

Table 10.4 *Drag calculations*

1.3 WING GEOMETRY SIZING

The actual wing area can be calculated simply as the take-off mass divided by the takeoff wing loading. But this wing area is the reference area of the theoretical, trapezoidal wing and includes the area extending into the aircraft centreline. Both values are found above and in previous study. Therefore;

Swing = W0/(W/S)0 = 1764.805/17 = 103.806ft^2 = 9.644m^2

The aspect ratio has been chosen as 7 before. The span of the wing can be found now:

$$b_{wing} = \sqrt{AR \times S_{wing}} = 26.96\,ft = 8.217m$$

We can find the root and tip chords by using the geometric equations below: Taper

$$C_{root} = 2S / b(1+\lambda) = 5.5ft = 1.677m$$

ratio (λ) has been chosen as 0.4 before;

$$C_{tip} = \lambda\, C_{root} = 0.6708m$$

Geometry	b (m)	C_{root} (m)	C_{tip} (m)	$\hat{C}$ (m)	$\hat{Y}$ (m)
Wing	8.217	1.677	0.6708	1.246	1.761

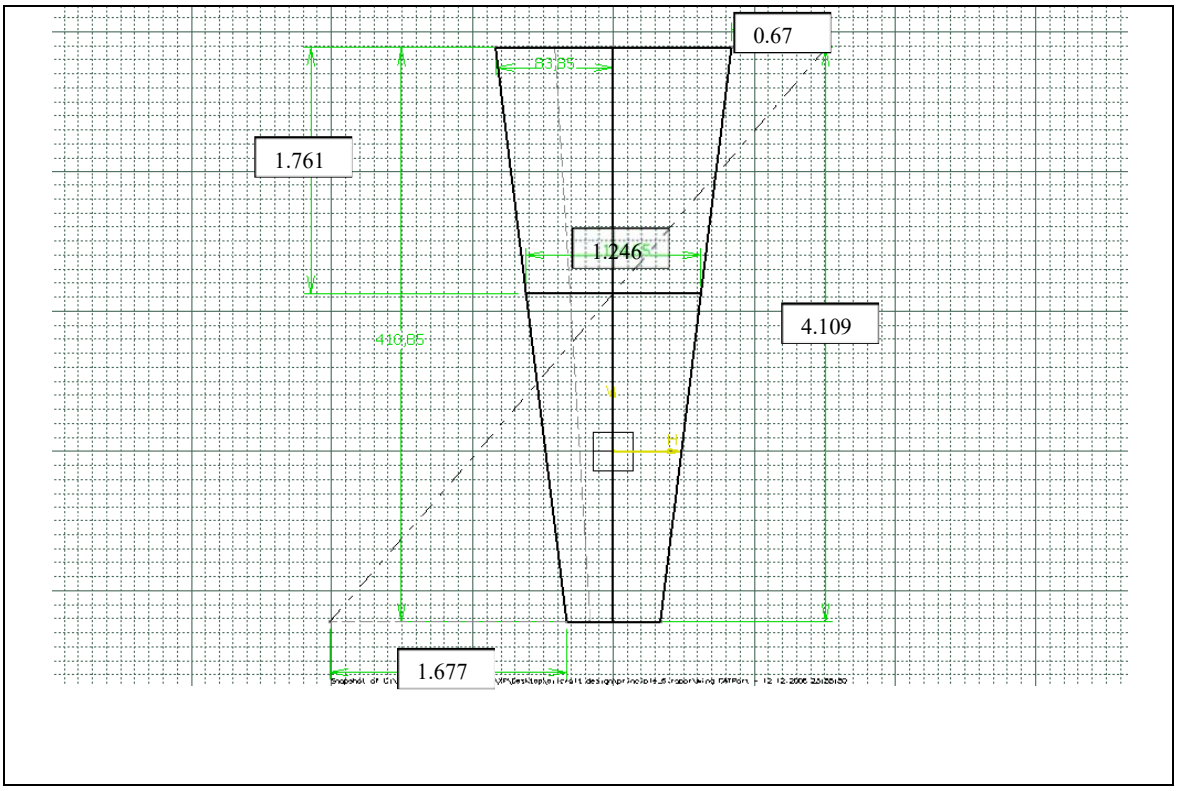

Figure 2 Top view of the wing

When the wing is designed, it is considered that the length of the entering part to fuselage as nearly 0, 30m. This part exists at the location of the maximum fuselage diameter. However, the aileron and flap lengths sums are approximately 3, 4m. After flap, there is 0, 42m to the fuselage. In order to not close the flap to fuselage, it is selected the distance between the flap and fuselage on wing is 0, 30m. Flaps, ailerons, elevator and rudder dimensions are determined in previous study "Initial Sizing".

Flaps: Flaps are placed on the wing which is 40% of the span and 24% of the chord.

$c_f / c_w = 0, 24$; $b_f / b_w = 0, 40$

$c_w = 1, 246m$ and $\mathbf{c_f} = 0, 24 \square 1, 246 = 0, 299m$

$b_w = 8, 217m$ and $\mathbf{b_f} = 0, 40 \square 8, 217 = 3, 2868m$ (For each wing = **1, 6434m**)

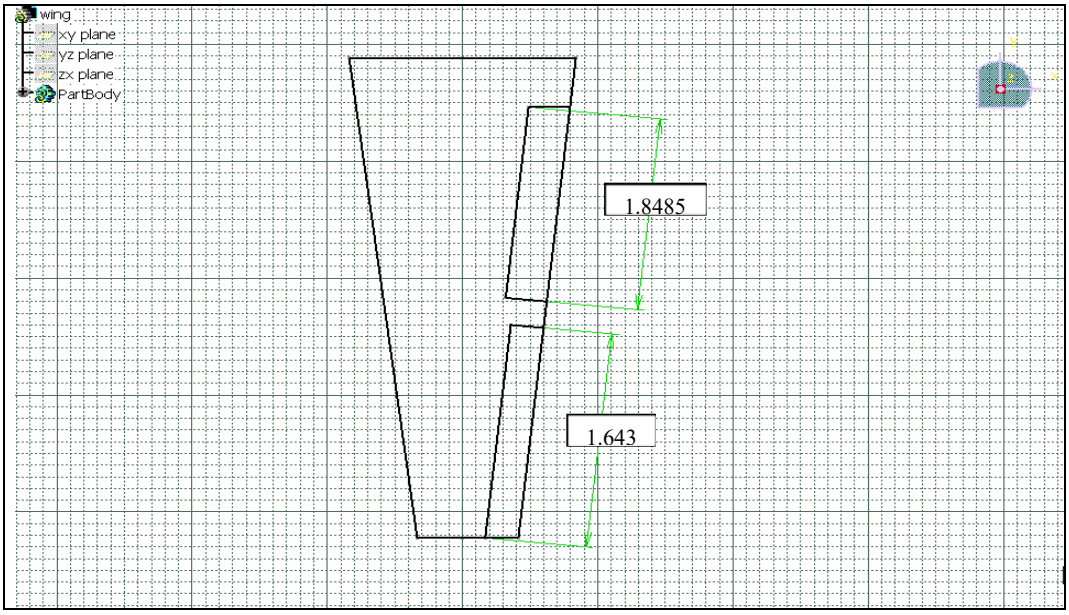

Figure 3 The sketch of the wing with flap and aileron

1.4 Location of Centre of Gravity Point

For a stable aircraft, the wing should be initially located such that the aircraft centre of gravity is at about 30% of the mean aerodynamic chord. When the effects of the fuselage and tail are considered, the centre of gravity would be about 25% of the total subsonic aerodynamic centre of the aircraft.

The mean aerodynamic chord of wing is 1, 246m. According to above information, the location cg point is 0, 3115m. The desired location of the cg point is shown in Figure4 below.

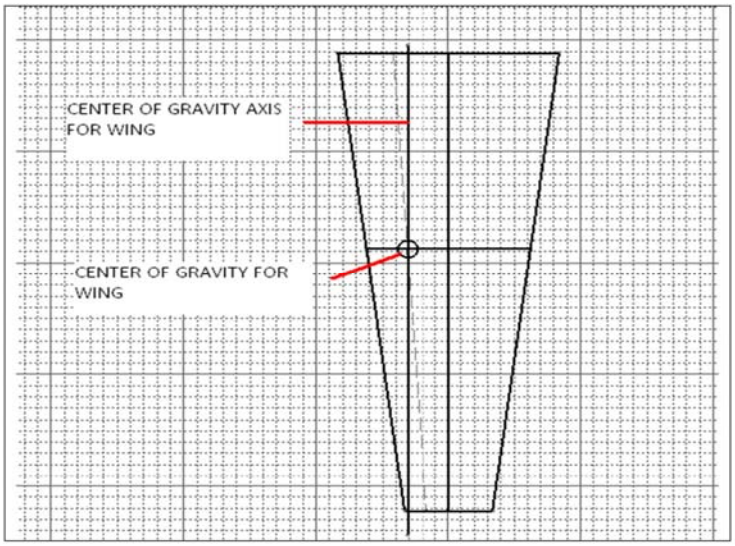

Figure 4 Location of C.G on the wing

1.5 Fuel System

Vtotal =2Vwing= 0, 155156m3

MTotal = (0, 85) (785) (0, 156) = 104, 1kg

This obtained value is really good value for this design. The required mission fuel mass is 98, 5kg. However, for integral tanks, there is foam in the wing to prevent fire and leak. This foam covers 2.5% of the volume. Also, 2.5% of the fuel is absorbed by the foam. When these losses are considered, remaining fuel is nearly the same the mission fuel.

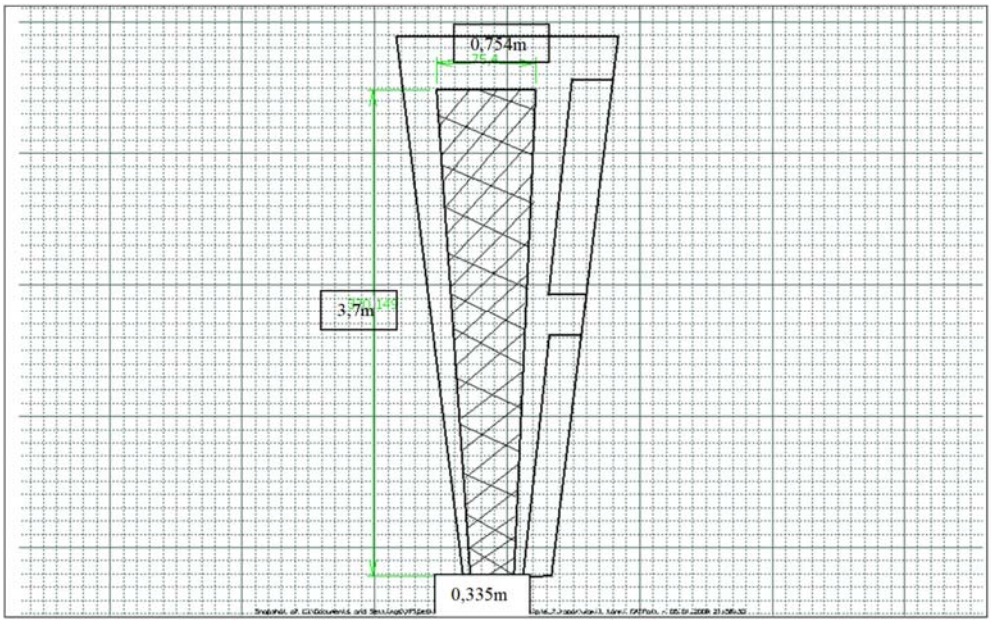

Figure 5 Fuel tank in the wing

1.6 Advanced Airfoils

Advanced transport technology studies show that supercritical airfoils can provide greater gains by increasing airfoil thickness and/or decreasing wing sweep at the same cruise Mach number, rather than by increasing cruise speed. Although increases in wing depth alone of approximately 30% can be used to reduce wing mass, it has been determined that the greatest benefit is achieved by a combination of increased depth, reduced sweep, and increased aspect ratio. The airfoil difference between a conventional (classical) and supercritical wing is shown in Fig. 8.1.6. The disadvantages of supercritical wing are:

- The incompatibility of the sharply "undercut" trailing edge with extensive flaps.
- The extremely close tolerances needed to maintain laminar flow.

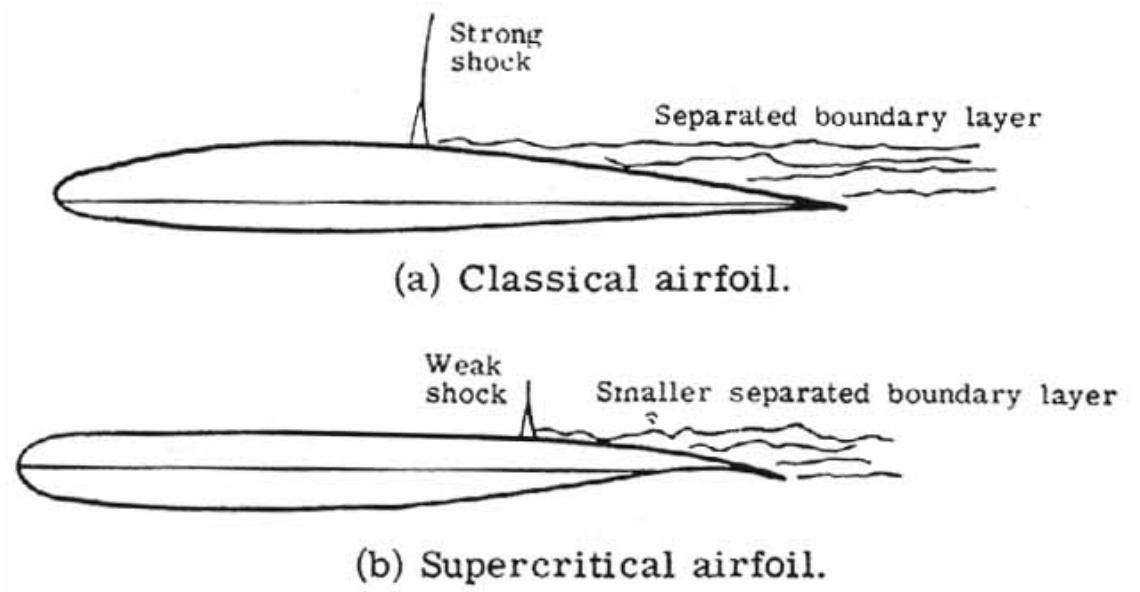

Figure 6 Conventional and supercritical airfoil comparison.

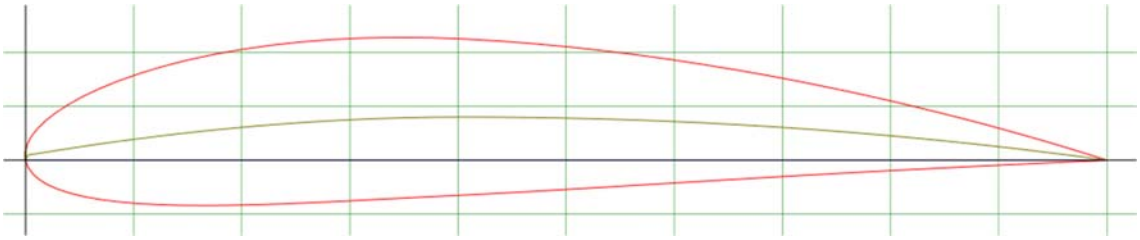

2 LITERATURE REVIEW

2.1 Introduction

The purpose of this is to explain the basic principles of wing design that can be applied to any conventional airplane. It will be noted that any wing requires longitudinal (lengthwise with the wing) members to withstand the bending moment which are greatest during flight and upon landing. This is particularly true of the cantilever wings, which are normally employed for high-per-formance aircraft. Light aircraft often have external struts for wing bracing, and these do not require the type of structure needed for the cantilever wing. But in our case, we will be considering a full cantilever wing without external struts. The outline of the wing, both in planform and in the cross-sectional shape, must be suitable for housing a structure which is capable of doing its job. As soon as the basic wing shape has been decided, a pre-liminary layout of the wing structure must be in-dicated to a sufficient strength, stiffness, and light mass structure with a minimum of manufacturing problems.

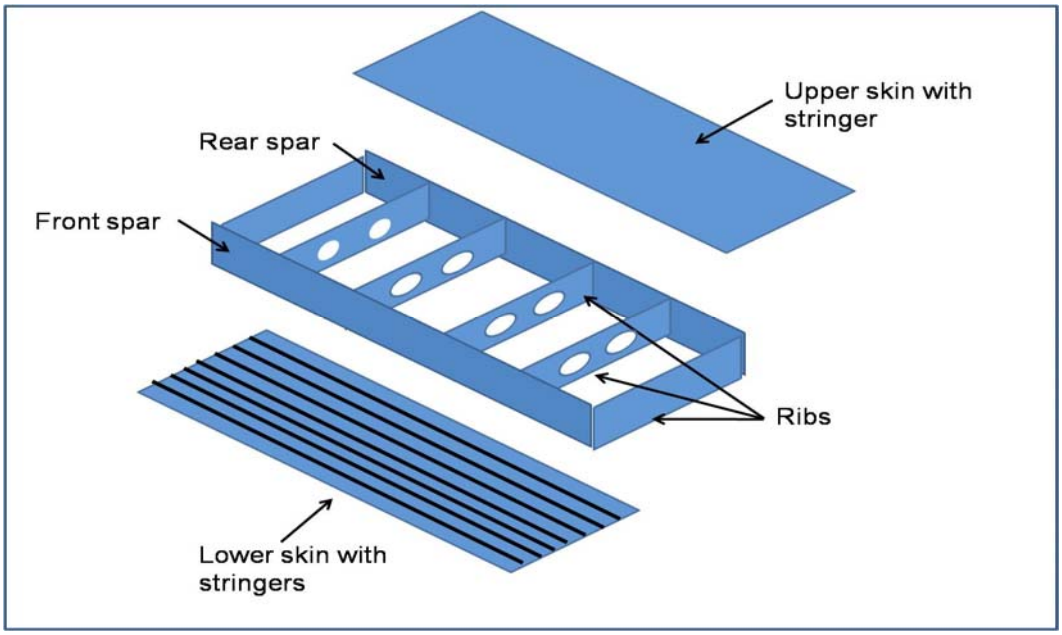

Figure 7 Wing box components (exploded view)

Elastic centrum: A point in the wing structure, in such a position that if the line of action of an imposed load passes through it, the load will cause no rotation of the cross section.

- Lift spar: A spar formed by two chord members connected by a web member, the chord members lying in a plane approximately perpendicular to the wing chord.
- Drag spar: A spar formed by two chord members connected by a web member, the chord members lying in a plane approximately parallel to the wing chord. [1]

[1] Ambri; Ramandeep Kaur. "Spars and Stringers- Function and Designing". Wing-box structure introduction.

2.2 Wing Box Design Properties

This shows how large percentage of the wing bending shall be carried by the spars and the stiffened cover. And the primary wing ribs will run normal to the rear spar. It is fairly obvious that the cover should be utilized for a large percentage of the bending material. Since torsional rigidity is required, this same torsion material may as well be used for both primary bending and torsion material. Spanwise stiffeners spaces fairly close together are, as a consequence, required to keep the buckling of the bending material down to a minimum.

It is noted that the torsion, shear, and bending are perfectly stable without the skin indicated area as A Further. it is perfectly stable to cut out all attachments and utilize only the skin to take out the torsion. Therefore, if both forms of structure are present, a consistent deformation analysis is required to determine the percentage of torque-carrying for each structure. For the center-of-pressure aft, the primary torque and the primary bending produce additive torsions which make this condition critical for torque in the wing root rib bulkhead. [2]

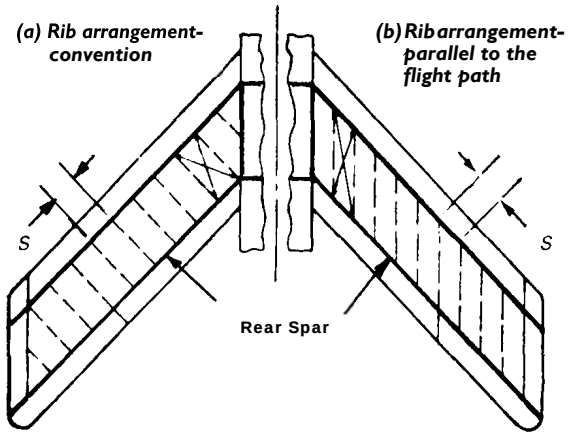

Figure 8 Comparison of rib direction (rectangular Box)

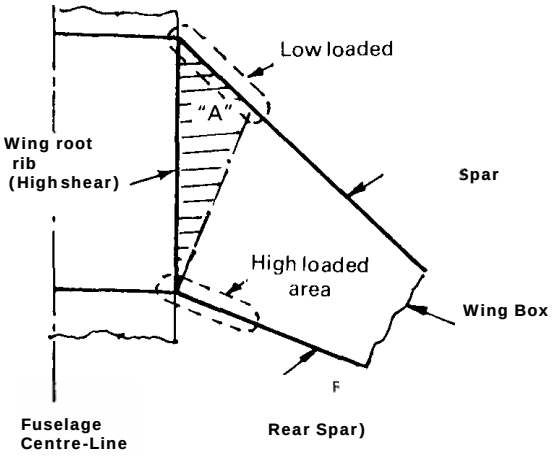

Figure 9 Wing root load distribution problem of swept wing (a high indeterminate structure)

[2] "Airframe Structural Design by Michael Niu" Airframe Structures. Published 1989.

2.3 Structural Calculation

This is to understand the formulation of the component structural formulas in a computational system. [3]

2.3.1 Tension Field Beam of Spar

The complete tension field behavior of the spar, which system is acted upon by a shear force $V=\frac{\partial M}{\partial Z}$. We would need to review its formulas.

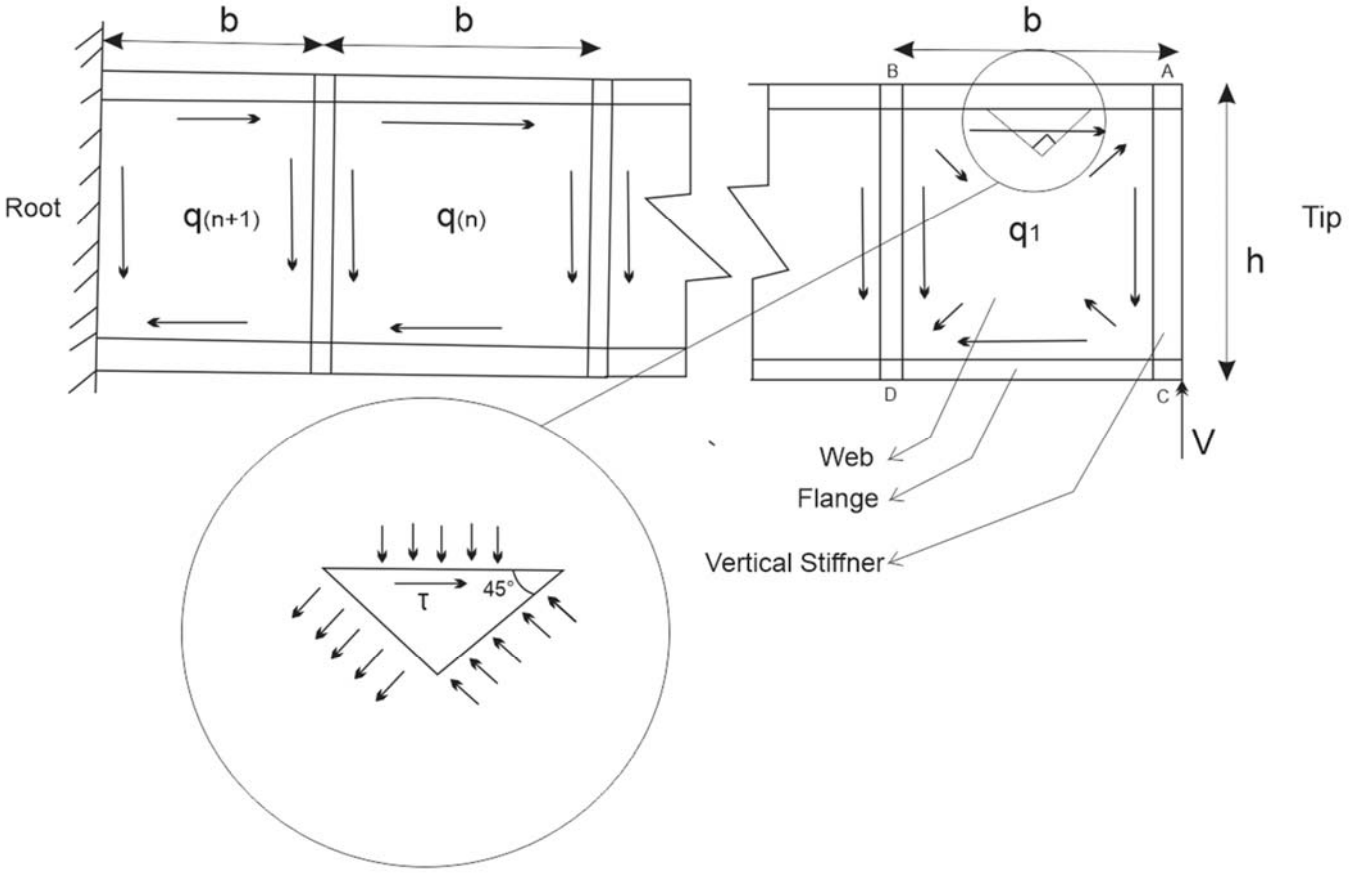

Figure 10 Tension Field Parameters of Spar beam

[3] T. H. G. Megson. "Aircraft Structures for engineering students". Published 2012

We know that shear flow distribution $\mathbf{q} = \boldsymbol{\tau}\,(t)$

Where, shear stress $\boldsymbol{\tau} = \frac{-V}{Ib}\int_{y1}^{y} ydA$ and t is the thickness

Therefore, $\mathbf{q} = \frac{-V}{I}\int_{0}^{s} ytds$

It is observed that shear flow distribution will be equal in a given web area for all surrounding stiffeners and flanges. But if a stiffener is bonded by two web regions the resultant shear force from both shear distribution must be calculated for that particular stiffener.

From the above figure, considering a small triangular element cut from the spar.

we can say that pressure force **P = f(t)(dx),**

Where **f** is the corresponding force, for tension $\mathbf{ft(t)}\left(\frac{dx}{\sqrt{2}}\right) = \mathbf{Pt,}$ and negligible for compressional force. The shear stress $\boldsymbol{\tau} = \mathbf{f_s(t)(dx),}$

Where the shear force $\mathbf{f_s} = \frac{V}{h(t)}$

Hence, we can examine the equilibrium state of the element

for $\sum fx = 0$

$\mathbf{Pt(cos45°) - \tau = 0}$

$\therefore$ $\mathbf{f_t = 2f_s}$

And for $\sum fv = 0$

$\mathbf{P_v - P_t\,(sin45°) = 0}$

$\therefore$ $\mathbf{f_t = 2f_v}$ (Where $\mathbf{f_v}$ is the vertical force)

These means, since $\mathbf{f_s = \frac{1}{2}q(b)}$ **or** $\mathbf{f_s = \frac{1}{2}q(h)}$

That tensional force, $\mathbf{f_t = q(b)}$ for flanges **or** $\mathbf{f_t = q(h)}$ for stiffeners

The above formula is understood to be utilized in FEA simulation of the spar structure.

2.3.2 Rib Cell Calculation

We know that the major function of ribs is to resist torsional loads. Hence, we will be considering only its torsional formulas.

Torque, $\mathbf{T = 2qA}$ (Where **A** is the cell area as shown below)

Twist Angle $\mathbf{B} = \frac{q}{2AG}\int_0^L \frac{ds}{t}$ (Where $\mathbf{G} = \frac{\tau}{\gamma}$ is the Shear Modulus) From the above

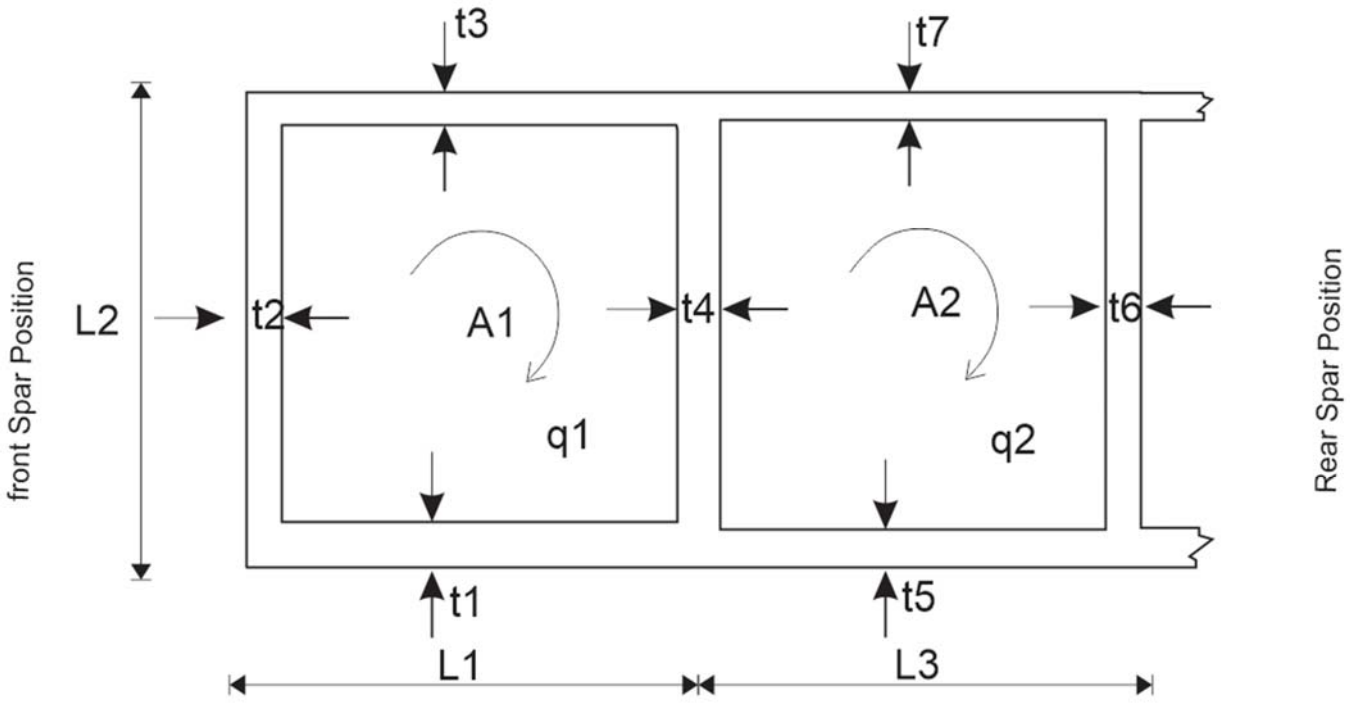

Figure 11 Cell dimensional parameters of a Rib

figure, as the rib cell (inner boundary) range from the front spar position towards the rear spar position, we know that the following formulas will be applicable;

$\mathbf{B = B1 = B2}$

Where, $\mathbf{B1} = \frac{1}{2(A1)G}\{q1(\frac{L1}{t1} + \frac{L2}{t2} + \frac{L1}{t3}) + (q1\text{-}q2)(\frac{L2}{t4})\}$

And, $\mathbf{B2} = \frac{1}{2(A2)G}\{q2(\frac{L2}{t6} + \frac{L3}{t5} + \frac{L3}{t7}) + (q2\text{-}q1)(\frac{L2}{t4})\}$

$$T = 2(q1)(A1) + 2(q2)(A2)$$

These patterns of formula will be repeated for n-number of cells for a given rib. To obtain its shear flow distribution and twist angle for a given torsional force (torque).

2.4 Wing-box Manual Load Calculation

This Literature show the load distribution of wing-box through manual method in Patran Software. And the extraction of IJES file type from Catia software. [4]

2.4.1 Extraction of Geometry

The assembly of parts of a wing-box structure were saved (extracted) to IJES file format in CatiaV5R20 and later imported individually to Patran Software. This extracted assembly file is shown below;

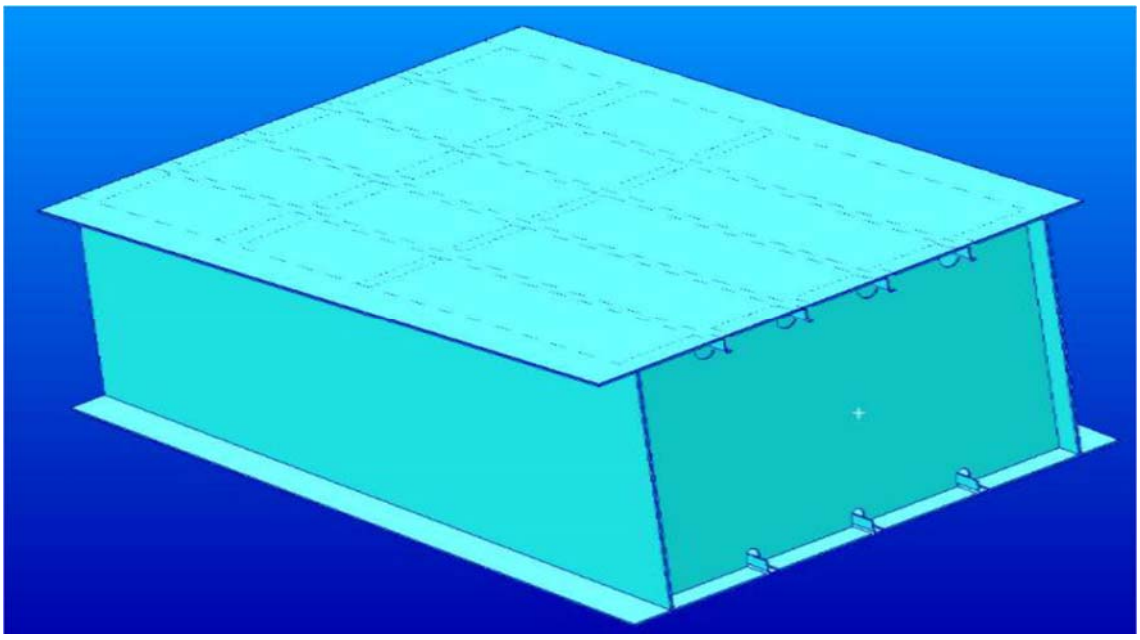

Figure 12 Catia IJES File Type Extraction

[4] Immanuvel D.; Arulselvan K.; Maniiarasan P.; Senthilkumar S. (2013). "Stress Analysis and Weight Optimization of a Wing Box Structure Subjected to Flight Loads". Weight optimization.

But due to the associative property of our future work we won't be making use of the IJES file format instead we will be using the CAT format.

2.4.2 Load Calculation

Considering the section enclosed within the planes AA and BB. Total span lenght of the wing is 7500 mm. But the span of the wing box section is taken as 1400 mm which is shown below;

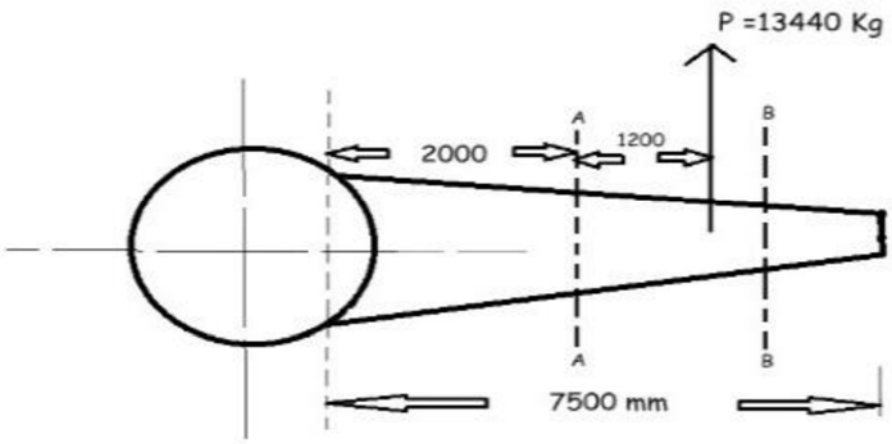

Figure 13 Section Wing Load Distribution

The following are the considered parameters;

Weight of the aircraft = 7000 k

Design load factor = 3.2 g

Design Factor of safety = 1.5

Hence, Total load acting on the aircraft = 33600 kg-f

We know that total lift load acting on an aircraft is assumed to be distributed 80 % and 20 % on the wings and fuselage respectively.

Hence, the total lift load acting on the wings = 26880 kg-f
This implies that the load acting on each wing = 26880/2 = 13440 kg-f
And total span for each wing = 7500 mm
The resultant load is assumed to be acting at a distance 3200 mm from the wing root (i.e. center of the fuselage). But this resultant load is actually at a distance of 1200 mm from the root end from section A-A of just the wing box, for analysis purpose. By this the bending moment of this resultant load can be calculated about the root end of the wing box from section A-A.
Therefore, bending moment = (13440)(1200) = 16128x103 kg-mm
Applied load at section B-B of the wing box = (16128)(103/1400) = 11520 kg-f
Total distributed load on the length of the tip end = udl * length,
Total distributed load on the length of the tip end = 4700 mm
Therefore, uniformly distributed load, UDL = 12649.41/4700 = 2.69 kg/mm

NB; For our future work we will make use of a much accurate load distribution on the wing box, since we understand that the actual real-life distribution of load is not uniform. Hence, we can simulate such real-life scenario using FSI of Ansys software.

2.5 Thickness Optimization with Abaqus

A typical thickness parametric optimization of wing-box skin using Abaqus software is described below. [5]

2.5.1 The model of the wing structure

Here Aluminum has been used only for the skin component while steel material is used for the remaining structural components. And the wing is made in a trapezoidal shape for ease of the analysis. Below is shown its dimensions;

[5] Zhengran Yang; Yi Jiang; Cong Huang (2014). "The Thickness of an Aircraft Wing Skins Optimization Based on Abaqus". Thickness Optimization.

Table 2. 1 Wing structure design size

Name	Section height	Chord	Wingspan	Tip chord	MB from LE	VB from TE	MB\VB length
Size/mm	250	1000	3310	700	200	200	1990

2.5.2 Finite Element Analysis and Thickness Optimization

Taking into account while ensuring the accuracy of the computation time and avoid unnecessary calculation, finite element model of an aircraft wing, of total division unit 8063. Constraints imposed are fixed wing at fuselage junction. Extraction of skin thickness at the design of the wing at the main premise of 10mm vibration mode, in which the low frequency vibration mode 5, and the high frequency vibration mode. Calculation and analysis show that when the skin thickness is 10mm, 1-order vibration mode, the frequency is 62. 027Hz, vibration mode maximum displacement is 1.01257mm, maximum Misses stress 82.206MPa, minimum Misses stress 0. 0870085MPa. It can be observed that as the wing bending and deformation at low frequencies are similar to the beam for its torsion characteristics. At higher frequencies, due to the re-arrangement of the wing and its material, the overall stiffness of the wing becomes small for the deformation of the wing skin and the rib vibration, when the skin thickness is 10mm, this phenomenon begins to appear from the first eight vibration modes. By the experiment's computational analysis, it is found that the wing skin thickness on each wing modal frequencies are different at each mode and this parameter has a different impact. Since the thickness of the skin is small, the deformation of the aforementioned wing will twist into the skin by the bending vibration of the rib, this phenomenon appeared earlier. Therefore, the thickness of the skin should not be too small. Taking into account the effects of skin thickness on the wing deflection, on the force, and modal frequency, but also taking into account the reliability of precision engineering process, so selecting the skin thickness of 8. 5mm - 9. 5mm for the experiment calculation and analysis will be feasible, the result is shown in the table below;

Table 3. 1 Wing parameter valuescalculated for each skin thickness

Skin thickness /mm	Maximum displacement/mm	Maximum stress /MPa	Minimum stress /MPa	Frequency /Hz	Appears rib vibration Order
8. 5	1. 01266	79. 7596	0. 0861964	61. 730	7
8. 6	1. 01265	79. 9298	0. 0854168	61. 754	7
8. 7	1. 01264	80. 0988	0. 0847865	61. 777	7
8. 8	1. 01264	80. 2668	0. 0842989	61. 800	7
8. 9	1. 01263	80. 4337	0. 0839471	61. 822	7
9. 0	1. 01262	80. 5996	0. 0837243	61. 844	7
9. 1	1. 01262	80. 7645	0. 0836232	61. 865	7
9. 2	1. 01261	80. 9284	0. 0836365	61. 885	7
9. 3	1. 0126	81. 0913	0. 0837569	61. 905	7
9. 4	1. 0126	81. 2533	0. 0839771	61. 924	7
9. 5	1. 01259	81. 4144	0. 0842901	61. 943	7

From the results it can be seen, that with the increase of skin thickness, the stability along the wing structure and the maximum displacement decreases, while the maximum stress increases and the frequency also increases. Also, it can be seen, that the smallest displacement between skin thickness 8. 5 ~ 9. 5mm decreases and then increases. But a difference is observed at skin thickness of 9. 1mm. As can be seen from the stress cloud, the maximum stress occurs in the body's location close to the main beam, the minimum stress occurs at the tip, as shown below. When preferred skin thickness, the need to minimize the maximum displacement of the wing and reducing the modal frequency of the wing, while avoiding excessive local stresses which is unreliable or can even damage the wing structure. Therefore, under the premises of this aircraft wing design, the preferred thickness of 9. 1mm is most appropriate.

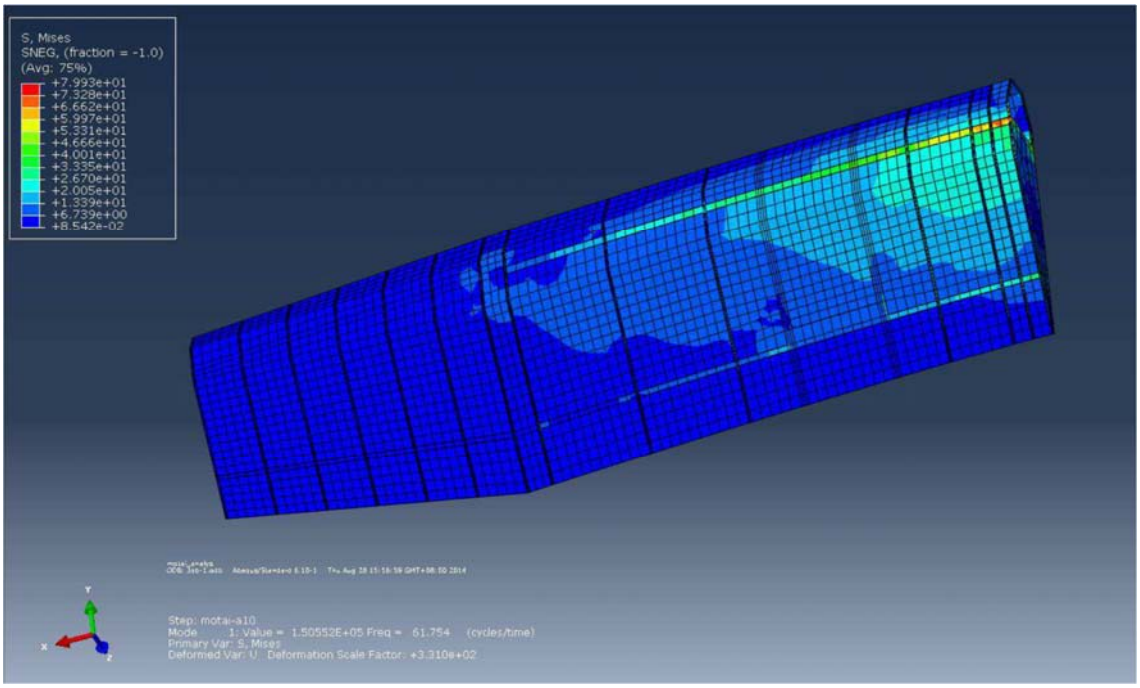

Figure 14 Abaqus Equivalent Stress Result

2.6 Spectrum Equation: Wing Tip Velocity Power Spectrum

This shows the final form of the output power spectrum due to a continuum of stationary, homogeneous, isotropic input as obtained from spectrum equation, which can be integrated numerically using the trapezoidal rule to yield:

$$\phi_w(s,w) = \phi_p(0,\omega) \sum_{j=1}^{N} Z_i Z_i + \sum_{j=1}^{N-1} \phi_p(j\Delta,\omega)\ 2\mathrm{Re}\left[\sum_{i=1}^{N-j} Z_i \bar{Z}_j\right] \qquad (47)$$

The result shows higher normalized spectrum power for lower frequencies of the atmospheric turbulence for frequencies ranging from 0.001Hz to 1Hz. This range of frequencies also applies to the wing tip velocity normalized by the gust velocity at different location along the wing span, as shown below:

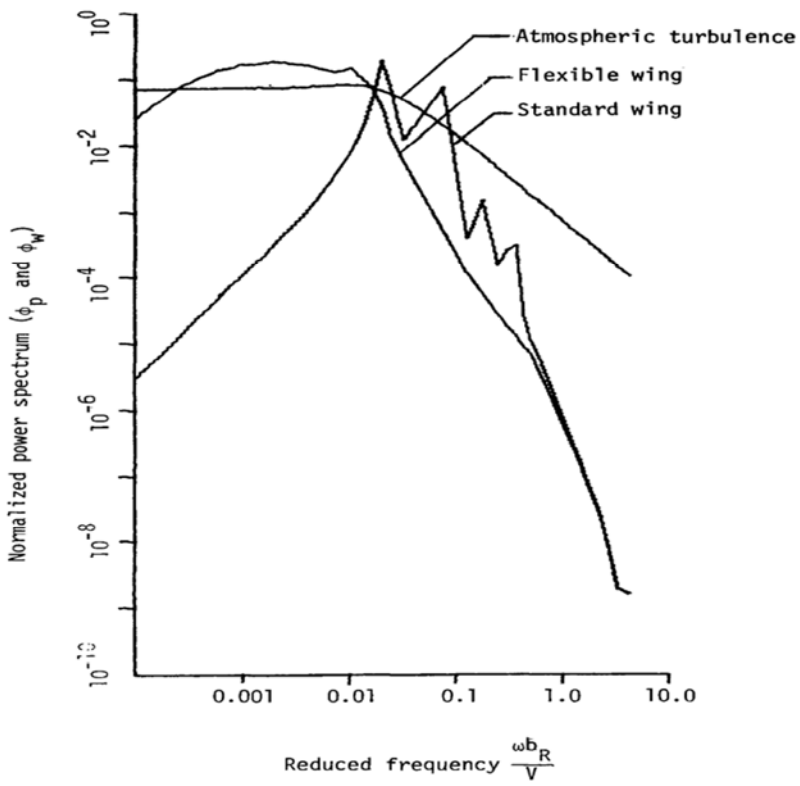

Figure 15 Spectrum of Atmospheric Turbulence for Length Scale 40.2m and Spectrum of Velocity at Wing Tip for Flexible and Standard Wings.

ϕw is the power spectrum of turbulence at wing tip and ϕp is the power spectrum of velocity at wing tip. [6]

[6] Robert L. Pastel; John E. Caruthers; Walter Frost (1981) "Airplane wing vibration due to atmospheric turbulence". Aircraft vibrating spectrum.

2.7 Conclusion

Vital information required for the wing-box design and evaluation has been carefully studied for a more effective result to our case study. Hence, we deduced that CAD will be used for our wing box design, of which a plain spar and rib beam (with no flange) will be used (i.e. to reduce parametric simulation difficulty). And also, the aforementioned manual approach to calculating the behavior of the wing-box structure will be replaced by computer aided FEA. In order to perform fluid (CFD) to structure coupled simulation and associative parametric modelling between it and the CAD.

We also understand that using values from the wing loading and aerodynamic forces data's, that the proper distribution of wind loads on the wing won't be of much accuracy. Hence CFD will be used to generate such loads to be transferred to the wing structure. The algorithm of this approach is shown below in form of a flow chart:

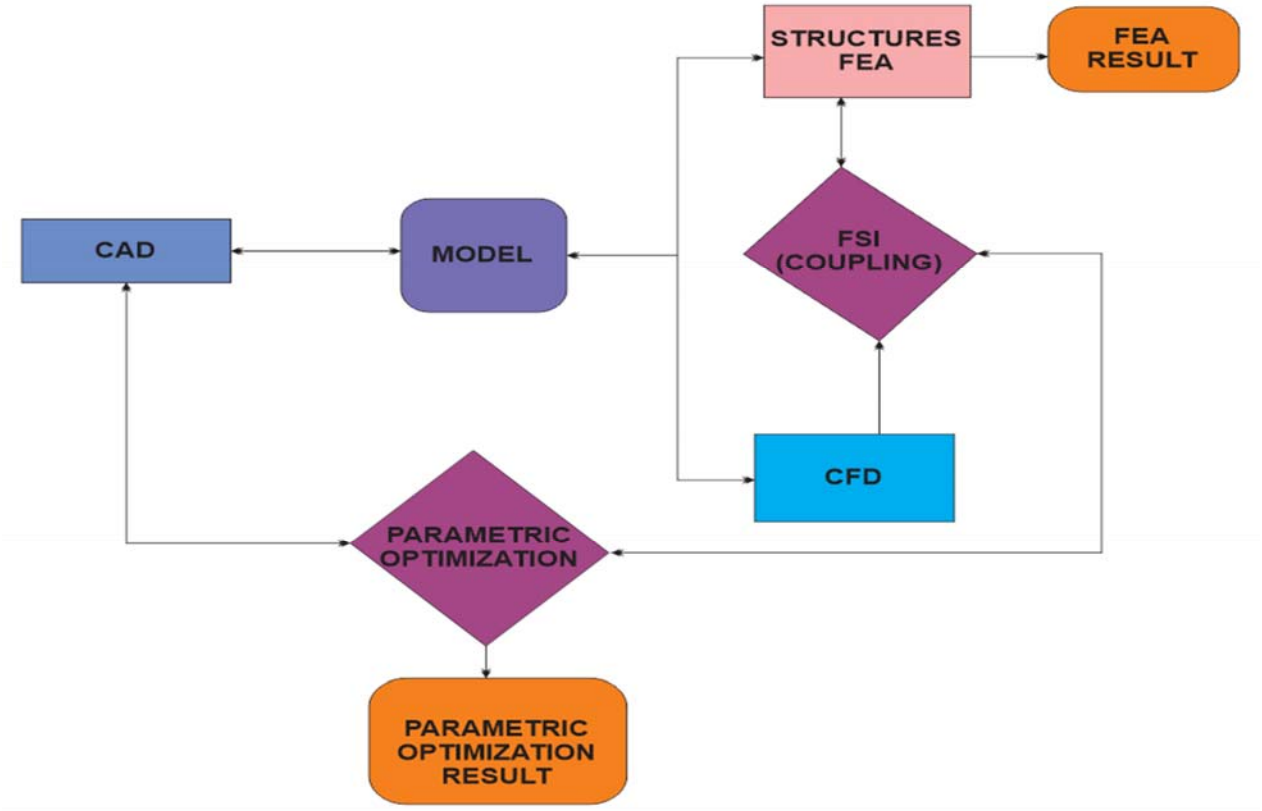

Figure 16 Project Flow Chart (Algorithm)

3 WING BOX CAD MODELLING

3.1 Introduction

The model of the conventional wing box for half span the full wing, is done using the Catia software. Its dimension was obtained from the previous aircraft design project on two-seater conventional aircraft which is also in the references list. A circular cross section was considered/modelled first for its stringers. So that in subsequent analysis, a different cross section can be considered and compared with the circular one, for better structural strength.

3.2 Parameters

Wing Sweep (L.E.) = 8.6°

Half Span, bwing/2 = 8.217/2 = 4.1085m

Root Chord, C_{root} = 1.677m

Tip Chord, C_{tip} = 0.6708m

Front Spar is located 15% of chord length from L.E.

Rear Spar is located 70% of chord length from L.E.

9 webbed rib with 410.67m spacing between each.

Circular stringers with 0.03m diameter. Stringers and its location on the cover surface at root chord (same ratio for the tip chord) are:

8 stringers on the bottom cover (between the two spars) with spacing of 0.10121m from the front spar.

8 stringers on the top cover (between the two spars) with spacing of 0.10145m from the front spar.

4 stringers on the L.E. cover with spacing of 0.10145m from the front spar

Airfoil NACA 4415

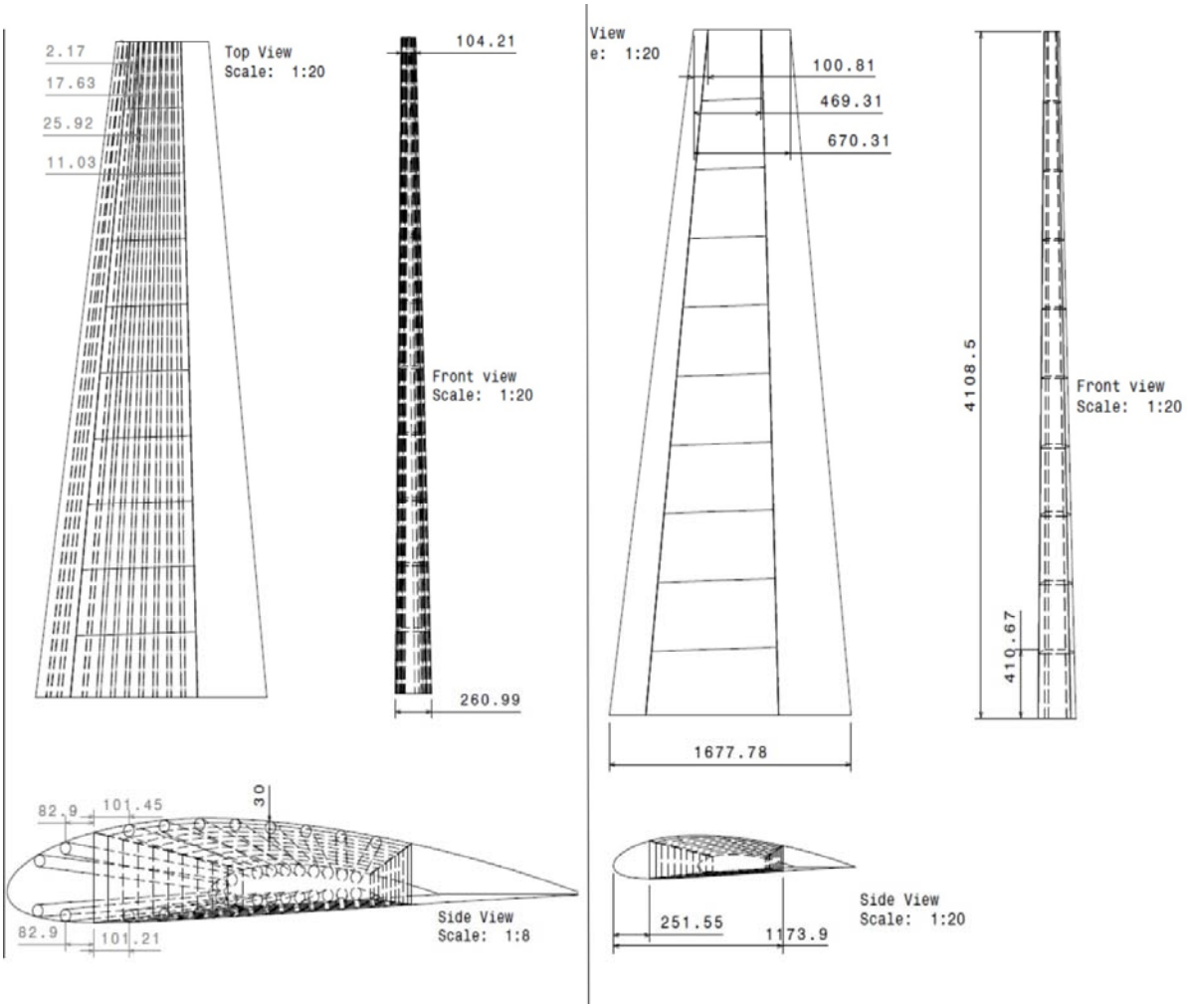

Figure 17 Model Dimensions

3.3 Procedure

- Open Catia V5
- Go to air-foil tool website, search and plot NACA 4415 for chord length of 1.677m and 0.6708m. Save both as .csv file.

- Open the first (root air-foil coordinate) .csv file in excel. Copy the x, y, z coordinate to 'GSD_PointSplineLoftFromExcel.xls', and run the micro to plot the air-foil spline and curve in Catia automatically.
- Repeat the above step for the second (tip air-foil coordinate) .csv file, but first edit it by adding 4.1085m to its z-coordinate and 0.1512m to its x-coordinate (obtained by 4.1085*(tan(8.6°))
- After the curves have been plotted I Catia. Using wireframe and surface design, extrude the root airfoil to the tip one (since it is a simple wing geometry with no kink, guide lines are neglected).
- Make two points for both root and tip chord line at 15% and 70% chord length.
- Extrude these lines to form the front and rear spar, up-to the cover surface.
- Draw 9 lines normal (perpendicular) to the rear spar up-to the front spar with equal spacing of 0.41067m
- Extrude these lines up-to the cover surface to form the webbed ribs.
- Sketch circles (18 circles) of 0.030m diameter both at the root and tip airfoil and make the constrained tangentially to airfoils. And make guide lines to join the circles spanwise sequentially at the tangential point.
- Use sweep feature to generate the tube-like stringer on the cover surface.
- Make and draft of the wing box with and without stringers, rendered iso view and other wireframe view with appropriate dimensions for top, front and side views.
- Save work and create a new part work
- The new part project is created by copy the old one. This is modified to produce a partially webbed rib, using the fill feature to an external (rib edges) and internal (Circular sections as shown below) boundary. These circles are tangential to an offset of 30mm from the rib edge. The spacing between the ribs are set using dependency formula as relation. This formula is dependent on the rib size:

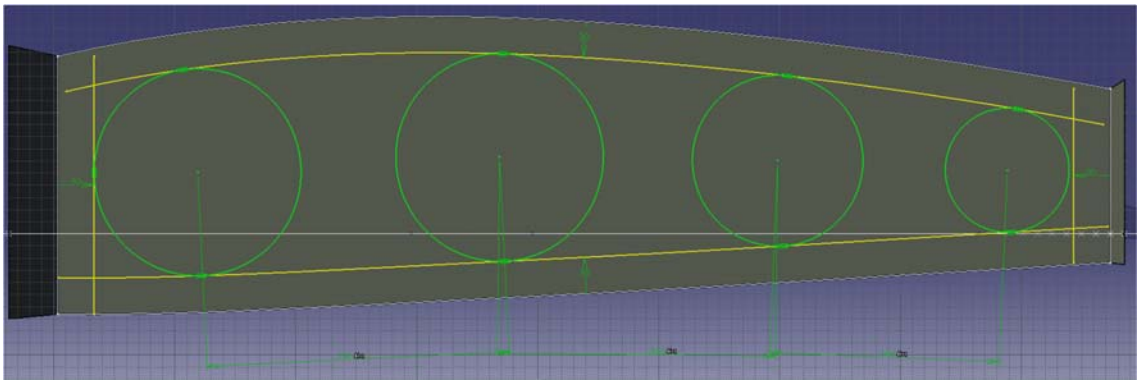

Figure 18 geometry for internal circular boundary of the rib\m

- Another partially webbed rib of circumscribed quadrilateral internal boundary is modelled, with the following geometry shown below. The quadrilaterals are tangential to the inertial circular boundary to make the comparative study between them, a relative value. But this is still constrained by the offset of the top and bottom edge of the rib. A corner of 10° arch is used to sharp the quadrilateral. Each constrain is created with a formula to help its replicability on all ribs.

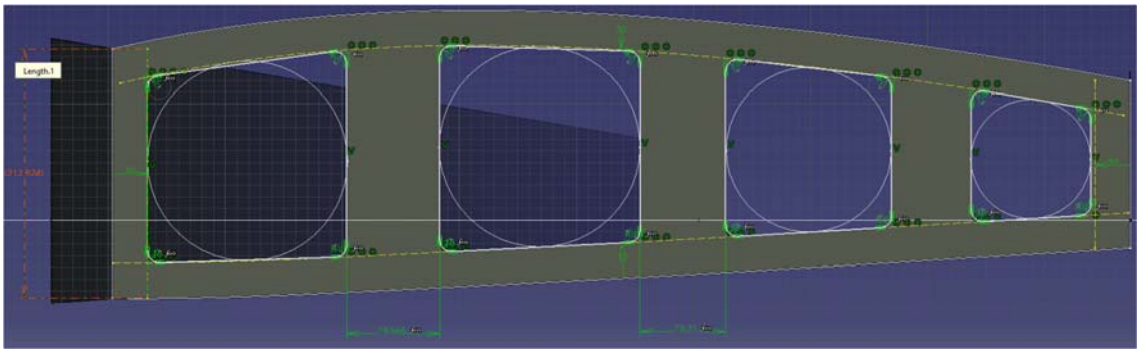

Figure 19 Geometry for internal circumscribed quadrilateral boundary of the rib

- Save work and exit

3.4 Modelled Result (Rendered View):

The modelled models are saved separately as .igs file format for the initial non-parametric comparison.

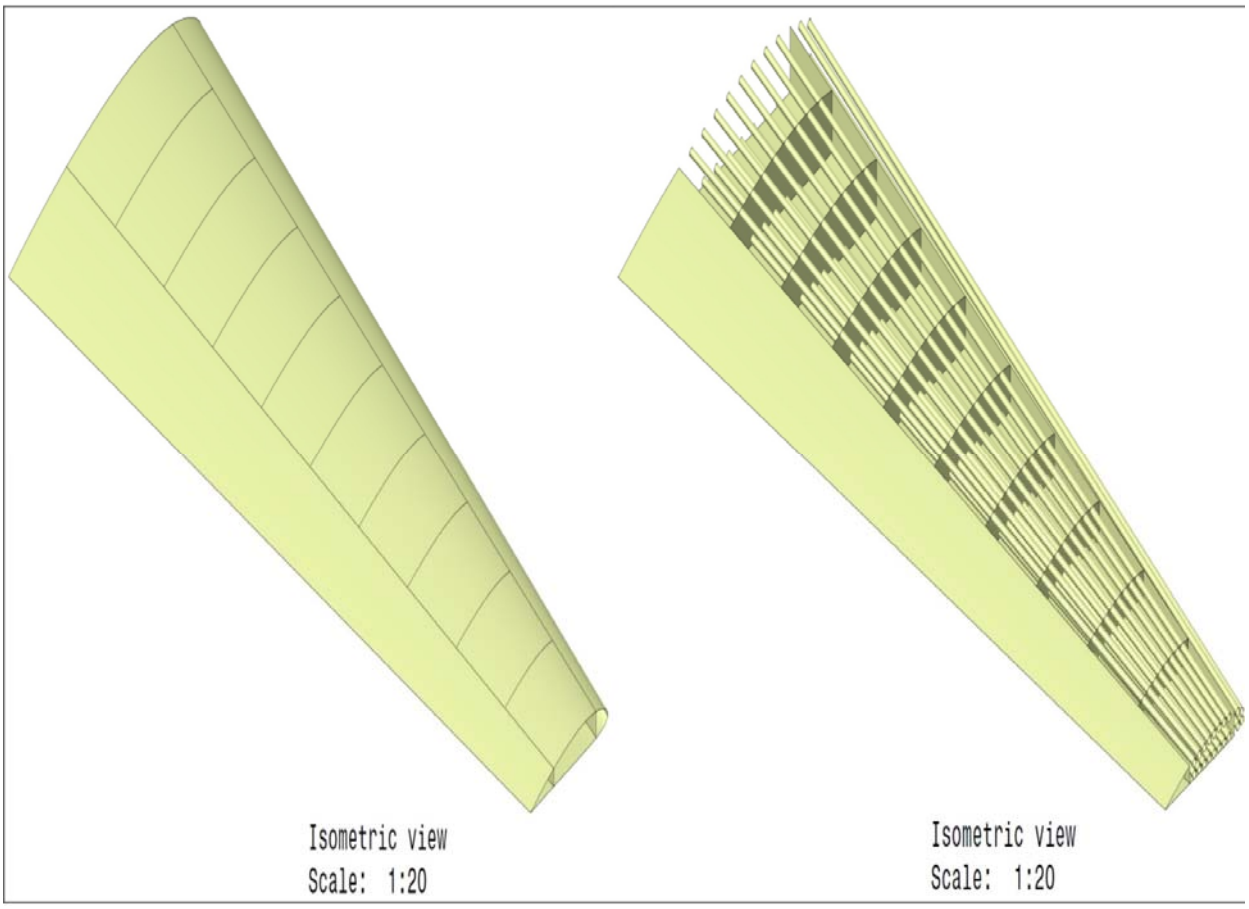

Figure 20 Wing-box model (rendered view)

3.5 Conclusion

The preliminary CAD design is done with the help of Catia V5 software. This modelled is initially done to analyze the importance of stringers, and other structural part of the

wing-box. In subsequent modelling the fuel tank will also be included with some adjustment to the wing box geometry.

4 COMPUTATIONAL WING BOX ANALYSIS

4.1 INTRODUCTION

The wing box structural validation is done using a coupled computational flow chart in Ansys software. This to ensure that the wing box structure is capable of withstanding the extreme cases of lift load/drag load during take-off and nose dive condition. And also, to with stand the mass of the wing load (due to fuels) on the ground. It is also important to note that when we speak of the structural strength of the wing box, we also refer to its bending/torsional strength. The Study is to be carried in different comparison cases, in other to obtain a better structural result.

4.1.1 Definitions and Nomenclature

- Included statically determinate structure: The part of a redundant structure which remains when enough of the redundant factors have been eliminated to make the remaining structure statically determinate.
- Beam force: A force parallel to the intersection plane of the lift spar web and Plane of symmetry
- Chord force: A force parallel to the plane which of the bisects the dihedral angle,

or the distance, between the planes of the two drag spars or trusses.

- Conventions for Signs:

Forces: An upward beam chord force is positive.

Moments: The torsional force is positive. A rearward moment cm the wing is a pitching. moment; therefore, we will consider a torsional moment positive. which tends to increase the angle of attack

4.1.2 Software Used:

- Ansys 17
- Catia v5

4.1.3 Project Schematic

For obtaining the force distribution on the wing, we needed to first get the pressure distribution on the wing first. For more reliable computation we have chosen an extreme wing load case during takeoff condition. These is carried out on the emphasis of validating the structural integrity of the wing, with and without stringers. A sample of the schematic diagram is shown below;

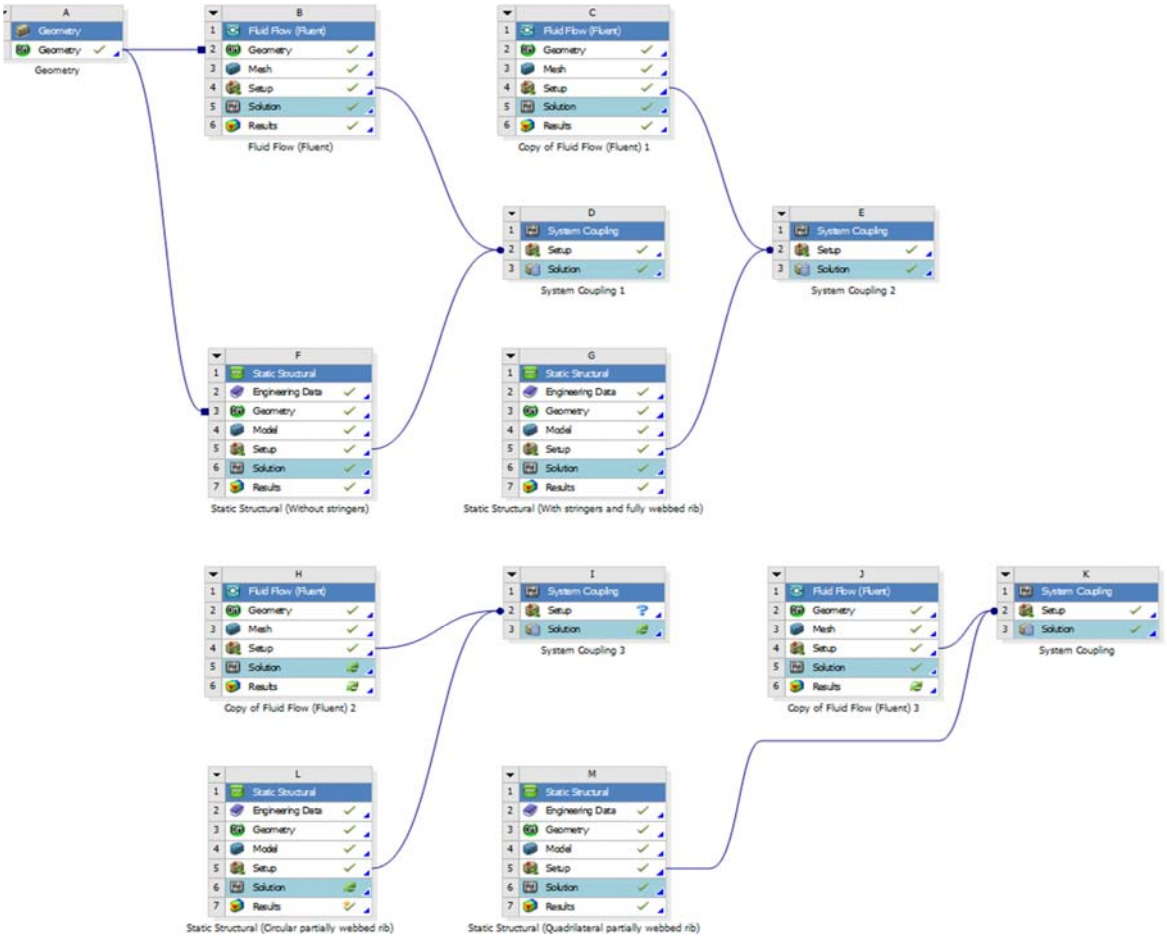

Figure 21 Project Schematics in Ansys

4.2 Materials Used

- Air is used as the working fluid in the fluent analysis, with the following properties;

Property	Units	Method	Value(s)
Density	kg/m3	constant	1.225
Cp (Specific Heat)	j/kg-k	constant	1006.43
Thermal Conductivity	w/m-k	constant	0.0242

Viscosity	kg/m-s	constant	1.7894e-05
Molecular Mass	kg/kmol	constant	28.966
Thermal Expansion Coefficient	1/k	constant	0

Table 1 Air Properties

- Aluminium is used throughout the entire static structural, because of its properties;

Material: aluminum (solid)

Property	Units	Method	Value(s)
Density(ρ)	kg/m3	constant	2719
Cp (Specific Heat)	j/kg-k	constant	871
Thermal Conductivity	w/m-k	constant	202.4
Young's modulus(E)	GPa	constant	70
Shear modulus	GPa	constant	26
Bulk modulus	GPa	constant	76
Poisson ratio(υ)		constant	0.35
Tensile Yield Strength	MPa	constant	280
Compressive Yield Strength	MPa	constant	280
Maximum Allowable Stress	MPa	constant	310
Shear Yield Stress(K)	MPa	constant	201.5

Table 2 Aluminum Properties

4.3 Generation of Pressure Force

The generation of pressure force and its distribution on the wing structure is done by using Ansys Fluent analysis software. To determine the overall behaviour of the fluid on the wing, of which is to yield maximum stress and moment. The following consideration for an extreme take-off scenario to validate the wing-box structural integrity, as are obtained from the previous project work;

Take-off velocity = 66.88m/s

Angle of Attack (AoA) = 15°

Box boundary domain = 7500*6000 *5000 for L*B*H respectively.

4.3.1 Creating Flow Geometry

- Open the Ansys workbench and import the 3D wing-box model from Catia software, as .igs file type. This is done on a single geometrical setup.
- The wing-box is rotated using the Body-transformation function to 15°
- By using DesignModeller we were able to create a box boundary domain and skin on the wing-box as shown below. Boolean subtract function is used to make the wing wall boundary. The boundary names are also shown;

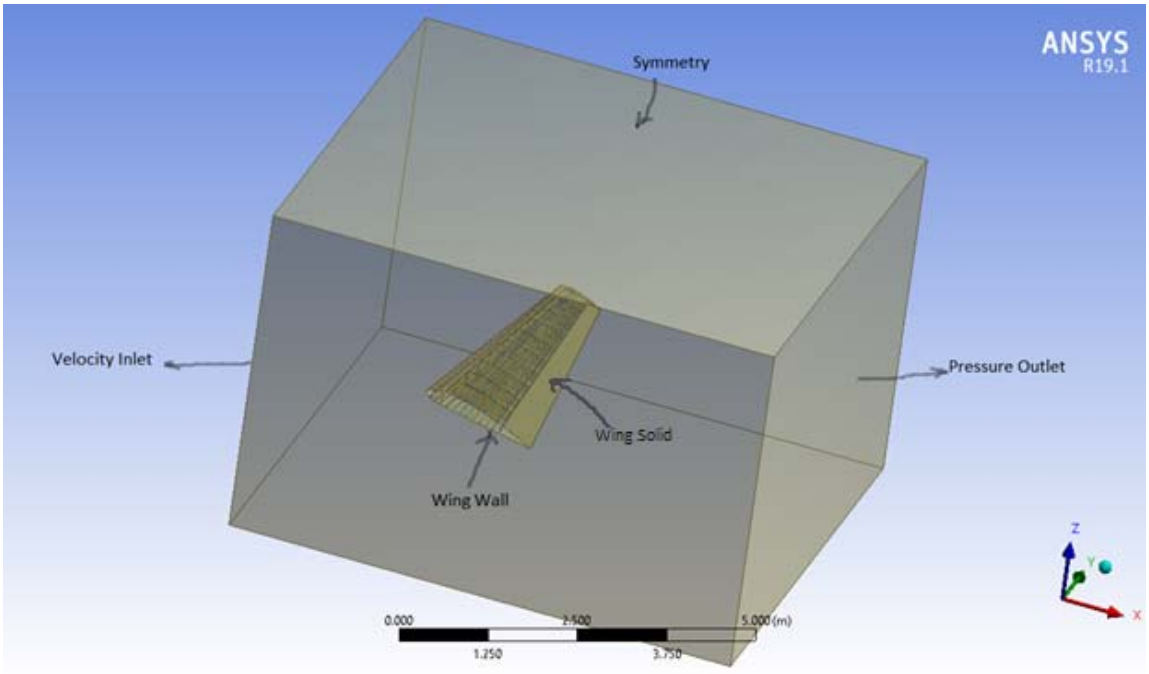

Figure 22 Boundary name selection-

4.3.2 Meshing and Setup

- Element size is 0.1m of 1 growth rate, with linear element order, to produce;

  Elements = 2099978

  Nodes = 2854990

- Boundary Conditions

Zones name	id	type
inlet	5	velocity-inlet
outlet	6	pressure-outlet
wall	7	wall
symmetry	8	symmetry
wing_solid	9	wall

- Laminar viscos model is used with operating conditions of gravitational acceleration set to -10m/s^2 on Z-component.
- Accordingly set the boundary conditions and reference is computed from inlet of 66.88m/s.
- Green-Gauss node base solver is used. Initialized to compute from inlet with absolute values.
- Run 100 iteration to obtain the converging values of lift, drag, pressure etc.

4.3.3 Result

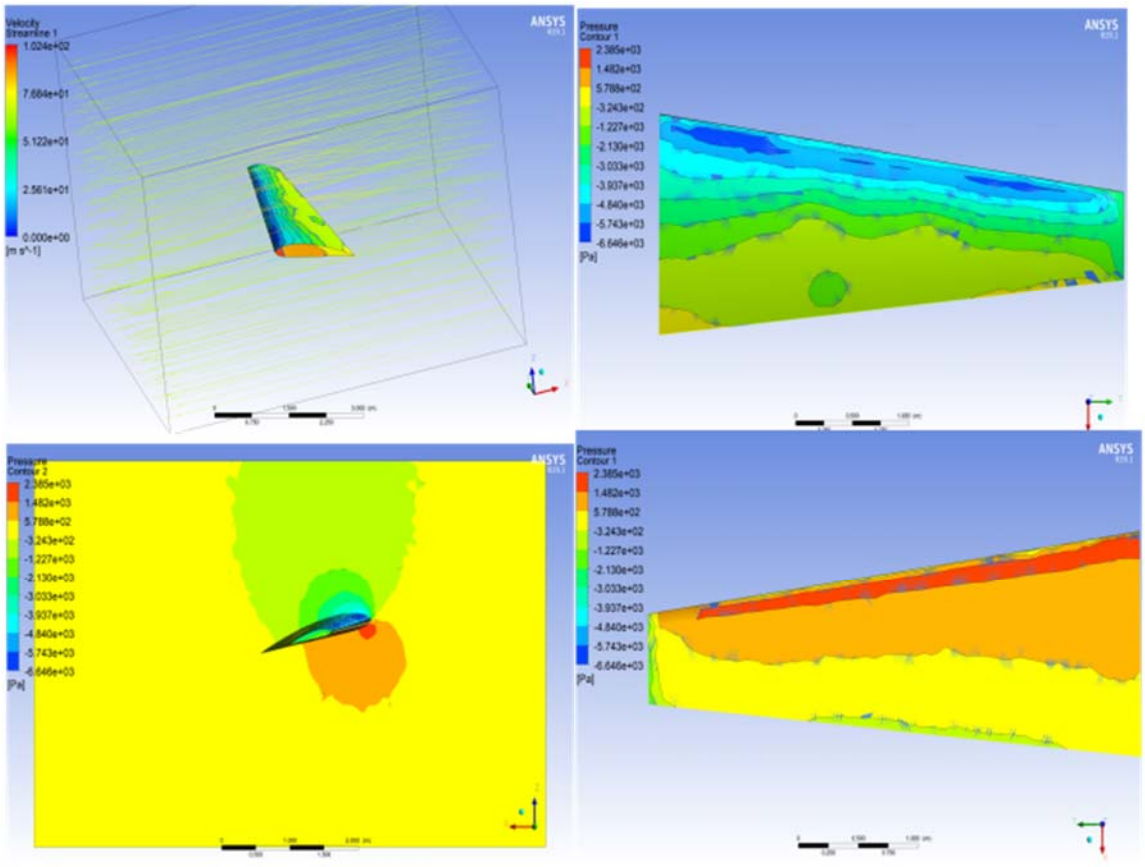

Figure 23 Fluid pressure force distribution on the wing

Result for the pressure force distribution is shown above, including the stream vector of the fluid. This is carried out at a condition when the aerodynamic for on the wing is maximum (i.e. at 15° angles of attack), to observe the worst-case scenario of the wing-box stability.

This result is coupled with the static structural system, in order to further analyse the wing box structure. The figure below shows the top and bottom pressure distribution contour with the velocity flow vector.

4.4 Static Structure Validation

4.4.1 Introduction

It is understood that von-mises equivalent stress defines the stress in a unit element of any cross section for its maximum compressive, tensile and shear strength, depending on the applied load on the overall structure. With this in mind the maximum von-mises stress will be obtained for tensile stress in Z-direction due to deformation in major in Z-axis. This maximum value obtained must be lower than 280MPa of aluminum tensile yield strength, because above this (elasticity) the material will act as plastic (plasticity).

Due to the impact of vibration of the wing by air particles it very important to observe the modal analysis of this structure, by obtaining the natural frequency of the wing-box in study. The modes are selected based on the anticipated frequency to be experienced by the flight mission. The obtained modal result can be further analyzed together with all applied forces in harmonic response analysis.

N/B: The geometry/mesh specifications used in fluent are used throughout the entire project

The analysis is done for wing-box without stringers and another with stringers. The results are compared side by side. The selected optimal result is further compared with a rib section of circular inner boundary. This is divided into different comparison study.

4.4.2 Structural Setup

Fixed support is set at the root rib of the wing, and the pressure force is applied as fluid solid interface through system coupling of fluent and static structural analysis, as shown below. As to be expected the coupling process is time consuming, hence a consideration of 4 iteration was appropriate to obtain a convergence. It is of great importance to consider the torsional deformation of the structure since we are studying the impact of skin stiffeners in this case. Hence directional deformation about the Y-axis of the wing-box centroid is included in the solution.

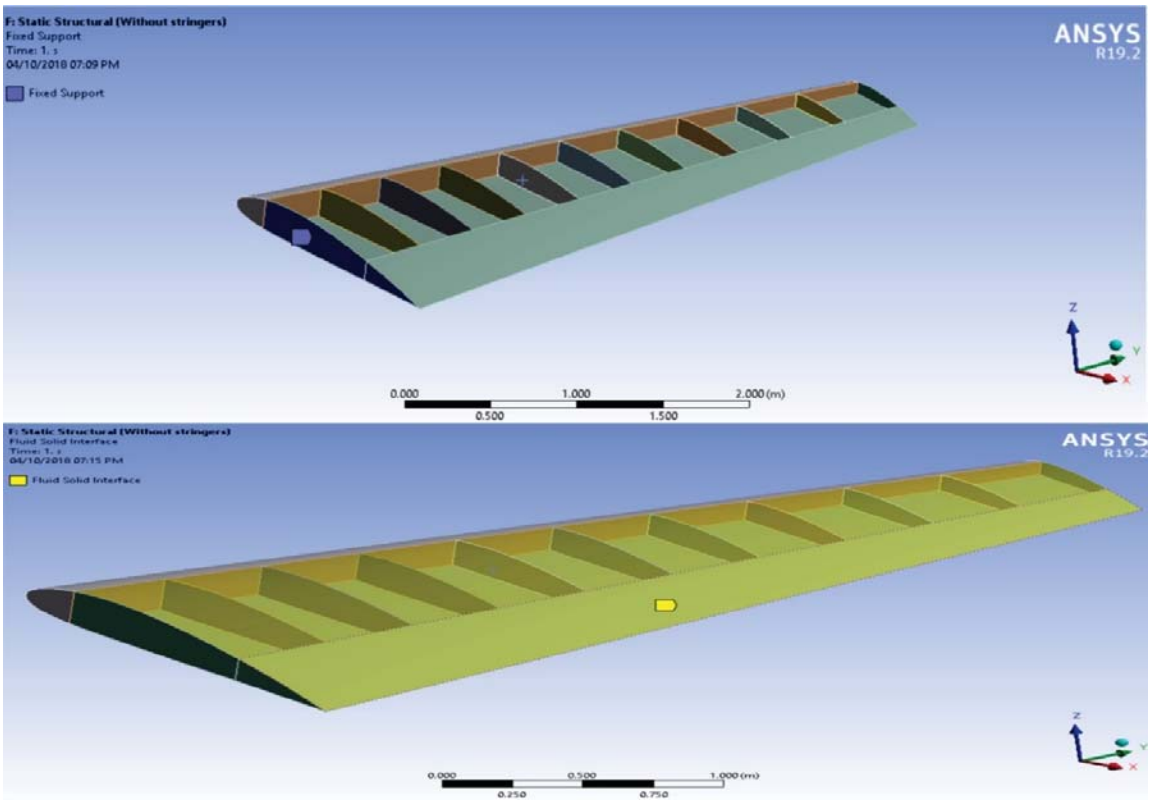

Figure 24 Load and support definition

The pressure force is applied through couple solution as fluid solid interface on the wing_solid boundary.

4.4.3 Coupling System

- Summary of System Coupling Setup

Unit System = MKS

- Initialization:

Option = Program Controlled (Starting from step/time equal to zero.)

- Step:

Option = Nondimensional Steps
Minimum Iterations = 1
Maximum Iterations = 5

- Duration:

Option = Number of Steps
Number of Steps = 1

- Data Transfer Information
  - Source: Copy of Fluid Flow (Fluent)

Region = wing_solid
Variable = force

- Target: Copy of Static Structural

Region = Fluid Solid Interface
Variable = Force

- General Information:

Name = Data Transfer
Execute Transfer At = Start of Iteration
Convergence Option = RMS Change in Data
Target Value = 0.01
Under Relax. Factor = 1
Ramping = None

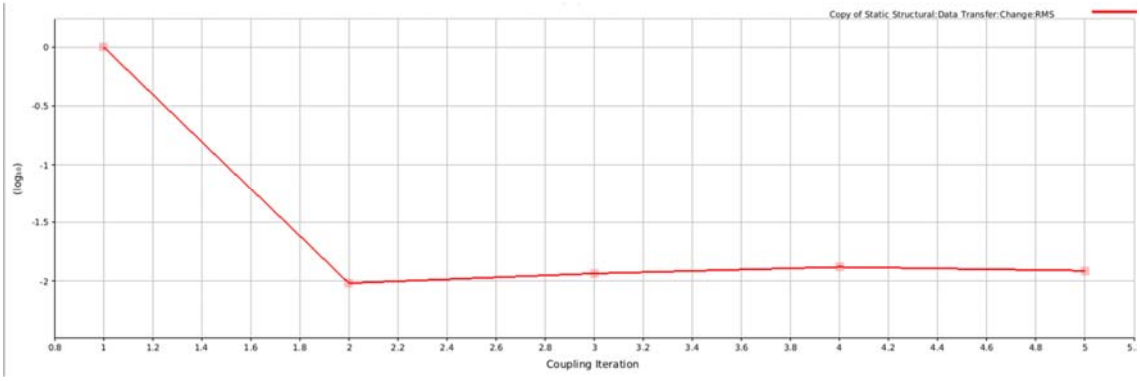

Figure 25 Logarithm vs. Coupling Iteration

4.4.4 Comparison Case Study One

The comparison of static structural solution for wing-box with stringers and without stringers is carefully described below.

4.4.4.1 Equivalent Stress (Von Mises)

Conditions	Minimum [Pa]	Maximum [Pa]	Average [Pa]	Mass [kg]
Without stringers	0.	3.6259e+007	8.5011e+006	215.05
With stringers	0.	1.2647e+007	1.6222e+006	322.43

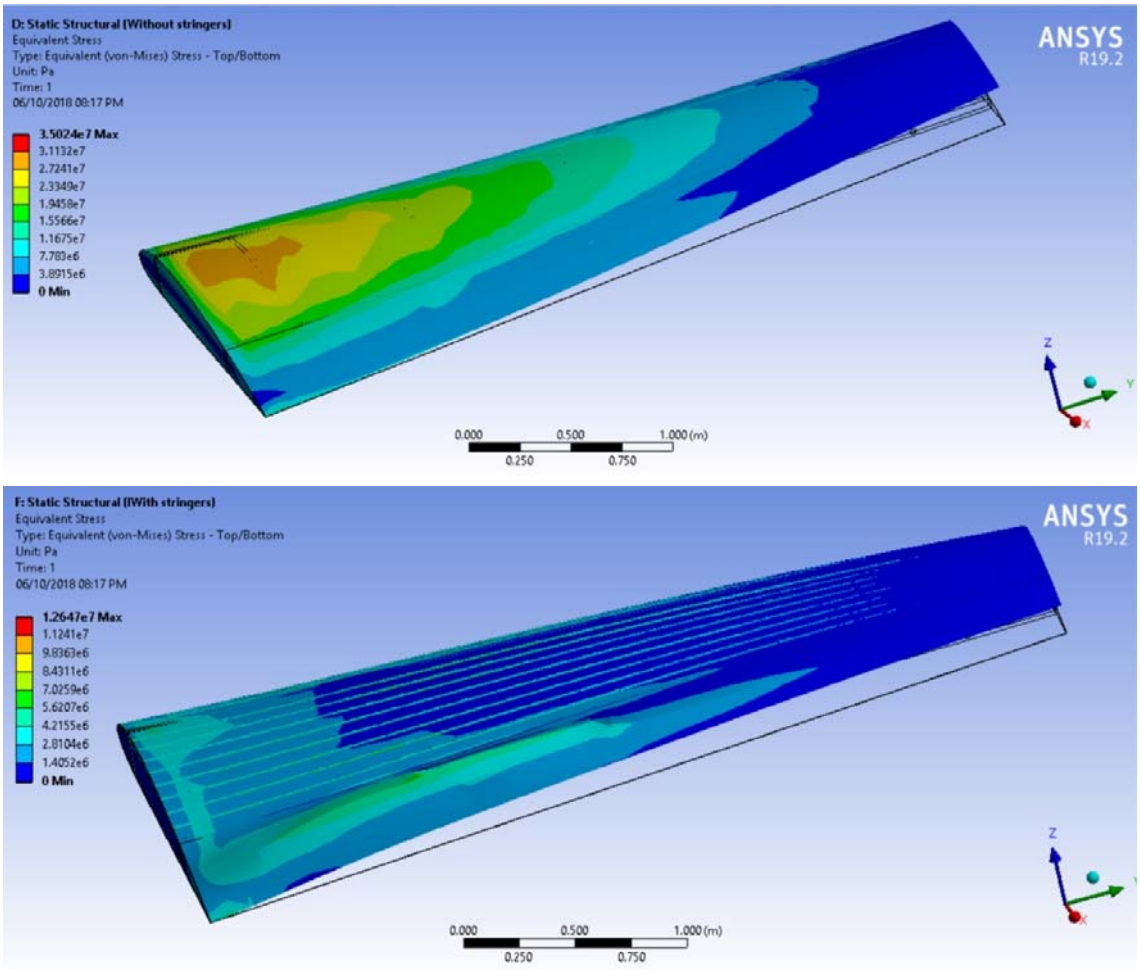

Figure 26 Equivalent Stress (von mises) case1

Both structural conditions have valid structural strength and integrity since their maximum (von mises) stress is less than the yield strength of aluminum (280 MPa), as shown above. The optimizing factor will be its mass to average stress ratio, which are;

For without stringers condition = 215.05/8.5011e+006 = 0.25297e-006 kg/Pa

For with stringers condition = 322.43/1.6222e+006 = 1.98761e-006 kg/Pa

Hence, it is observed that the condition with stringers has better mass to strength performance. Fulfilment of this purpose is shown as the minimum to maximum torsion is very minimal for the condition with stringers as compared to the condition without stringers. This is our primary focus for the selection of wing-box CAD geometry.

4.4.4.2 Total Deformation

Conditions	Minimum [m]	Maximum [m]	Average [m]	Mass [kg]
Without stringers	0.	2.0116e-002	8.1037e-003	215.05
With stringers	0.	1.988e-003	4.3145e-004	322.43

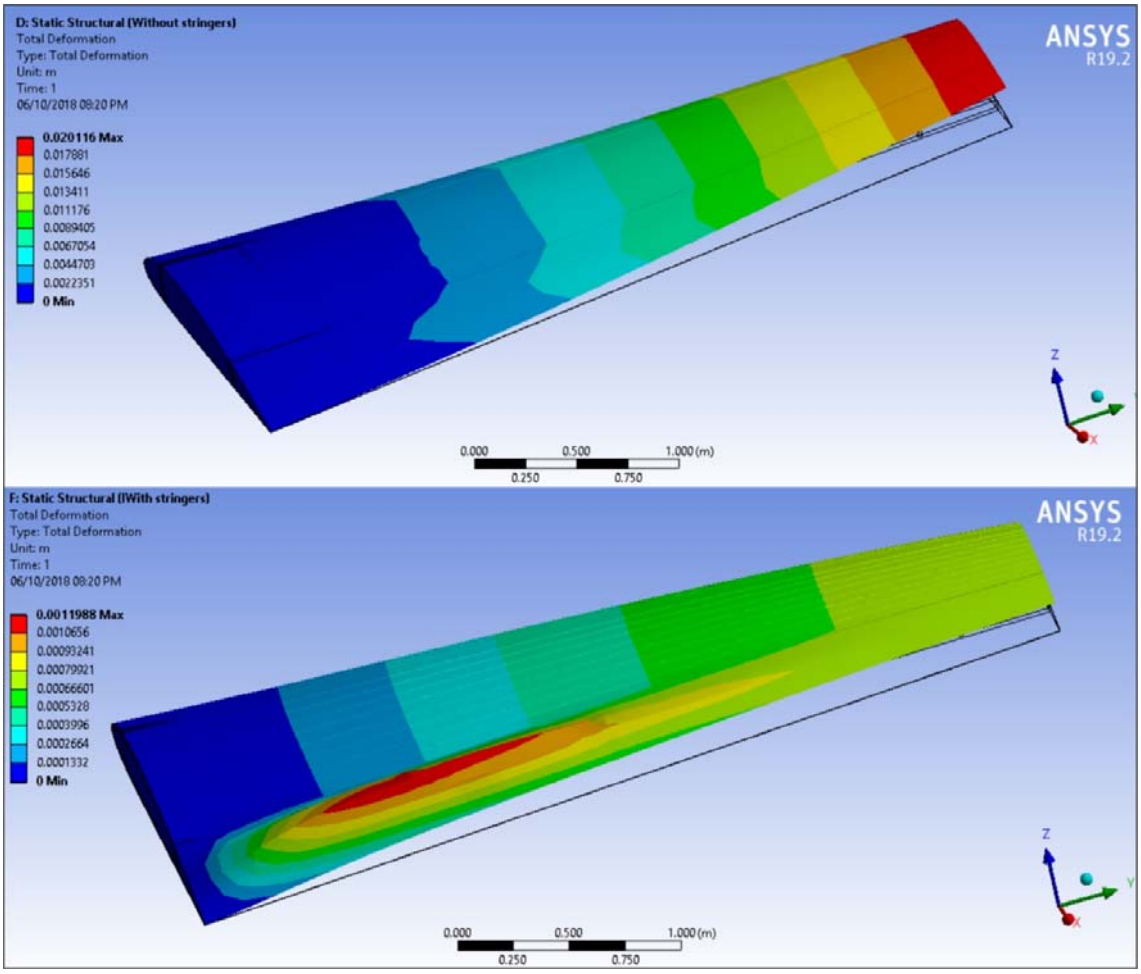

Figure 27 Total Deformation case1

The bending in z-direction due to the lift force causes deformation. The deformation is very low in both conditions but is better with the condition with stringers since the maximum deformation is 1.988 mm at the trailing region.

4.4.4.3 Torsional Deformation (Directional)

Conditions	Minimum [m]	Maximum [m]	Average [m]	Mass [kg]
Without stringers	-5.0167e-004	5.1978e-004	1.1857e-004	215.05

With stringers -2.5645e-005 2.8731e-005 3.299e-006 322.43

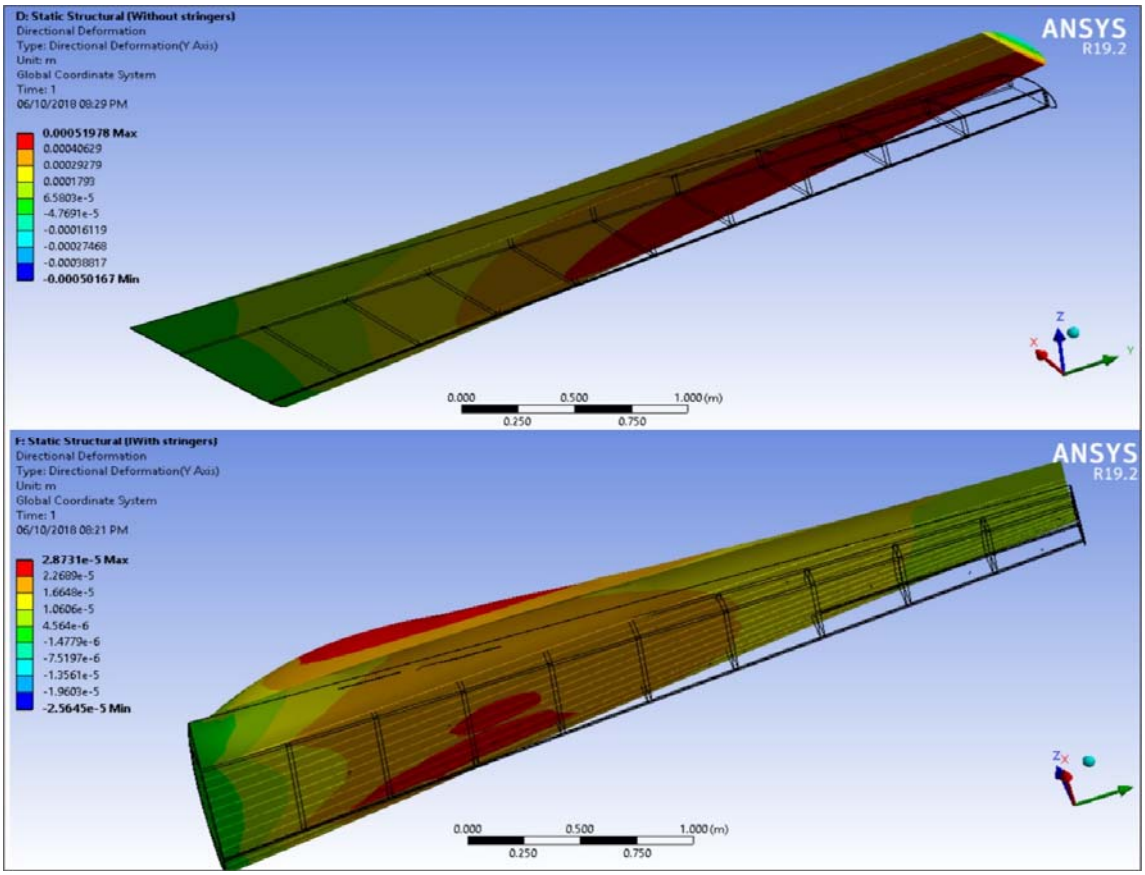

Figure 28 Torsional Deformation case1

Directional deformation about the y-axis of the wing-box centroid is considered for it torsional deformation (twist). To increase the structural strength of the wing skin is the primary purpose of the stringers (stiffeners). But this criterion is not considered for this comparison, due to the function of a stringer is to resist torsional deformation. Hence it is observed that the twisting is very less in the condition with stringers than that without stringers, as described in the above table.

4.4.4.4 Result

All important characteristic is taken into consideration while comparing both conditions. It can be observed that both conditions have its maximum equivalent (von mises) stress within the yield strength of aluminium, as shown in the above tables as 36.259 MPa and 12.647 MPa < 280 MPa for without stringers and with stringers respectively. These result in very low (tolerable) deformation (bending) and torsion, as shown in the above tables. The mass to average stress ratio is considered for optimal selection of one of these conditions as described above. Therefore, the Wing-box with stringers is selected for further optimization and re-modelling, because of its better resistance to torsional deformation, without considering its poor mass to stress ratio if compared with the other condition. This is done, because the primary purpose of stringers is to resist twisting of the wing surface, therefore we focused on just the torsion deformation parameter. Hence the validation of this structure is completed and observed to be within the acceptable range for its material and mission requirement.

4.4.5 Comparison Case Study Two

For this analysis we have chosen the wing-box with stringers and circular inner boundary rib section, to be compared side by side with wing-box with stringers and circumscribe quadrilateral inner boundary rib section. These will be tabularized in two conditions as circular webbed rib and quadrilateral webbed rib, respectively. The view is taken for different components of the wing box for observation purposes.

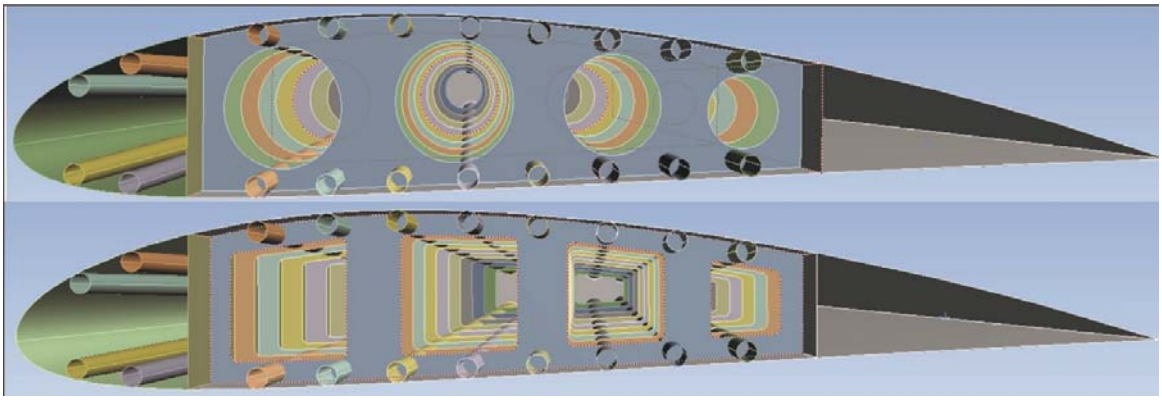

Figure 29 Partially webbed rib (wing-box model)

4.4.5.1 Equivalent Stress (Von Mises)

Rib Conditions	Minimum [Pa]	Maximum [Pa]	Average [Pa]	Mass [kg]
Circular webbed	0.	1.2408e+007	1.6225e+006	306.12
Quadrilateral webbed	0.	1.2102e+007	1.5278e+006	300.13

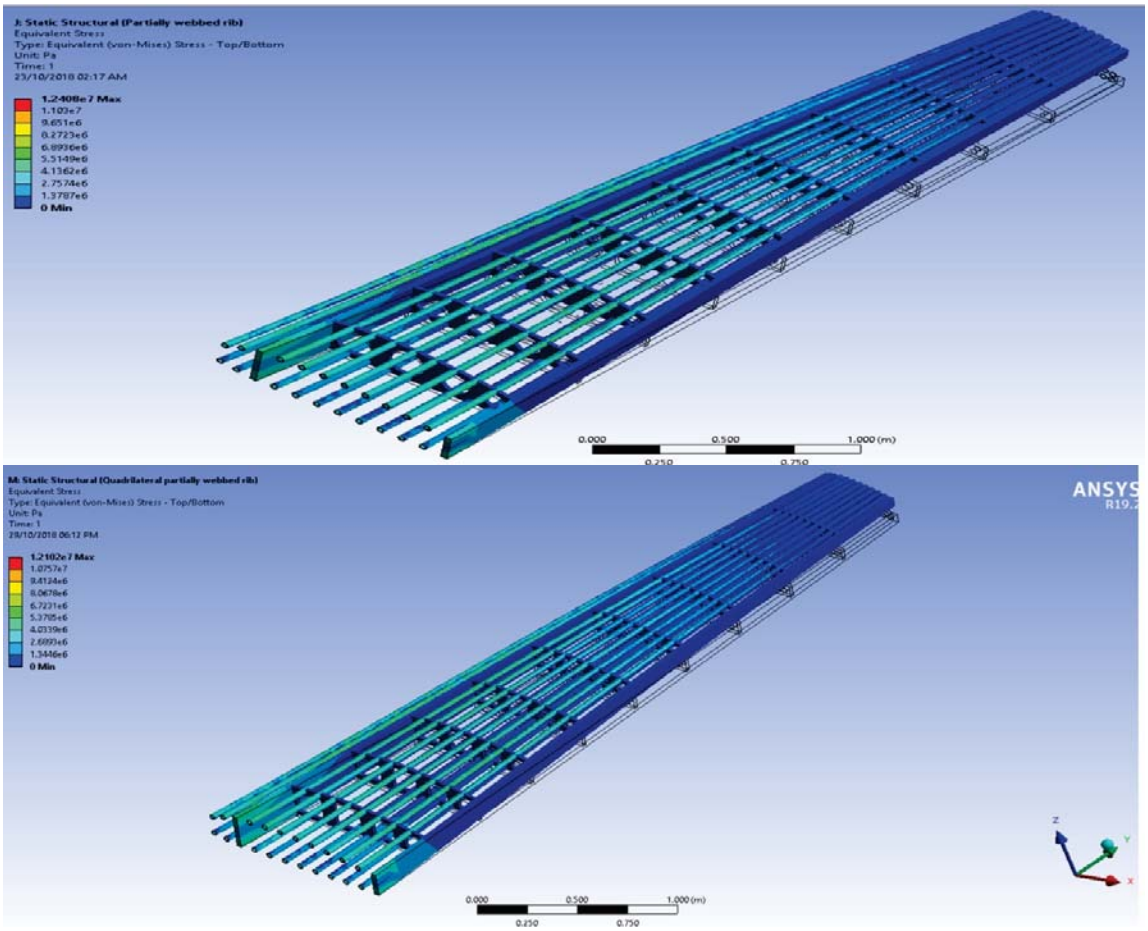

Figure 30 Equivalent Stress (von mises) case2

For this study, our primary focus will be on the mass to stress performance of these two conditions.

Calculating the mass to average stress ratio for the two conditions;

For circular webbed rib = 306.12/1.6225e+006 = 1.8871e-006 kg/Pa

For Quadrilateral webbed rib = 300.13/1.5278e+006 = 1.96361e-006 kg/Pa

The condition with Quadrilateral webbed rib is calculated to have slightly better stress to mass performance. This result is taken into consideration during the selection of the wing-box CAD geometry.

4.4.5.2 Total Deformation

Rib Conditions	Minimum [m]	Maximum [m]	Average [m]	Mass [kg]
Circular webbed	0.	1.2887e-003	4.3533e-004	306.12
Quadrilateral webbed	0.	1.4094e-003	4.2525e-004	300.13

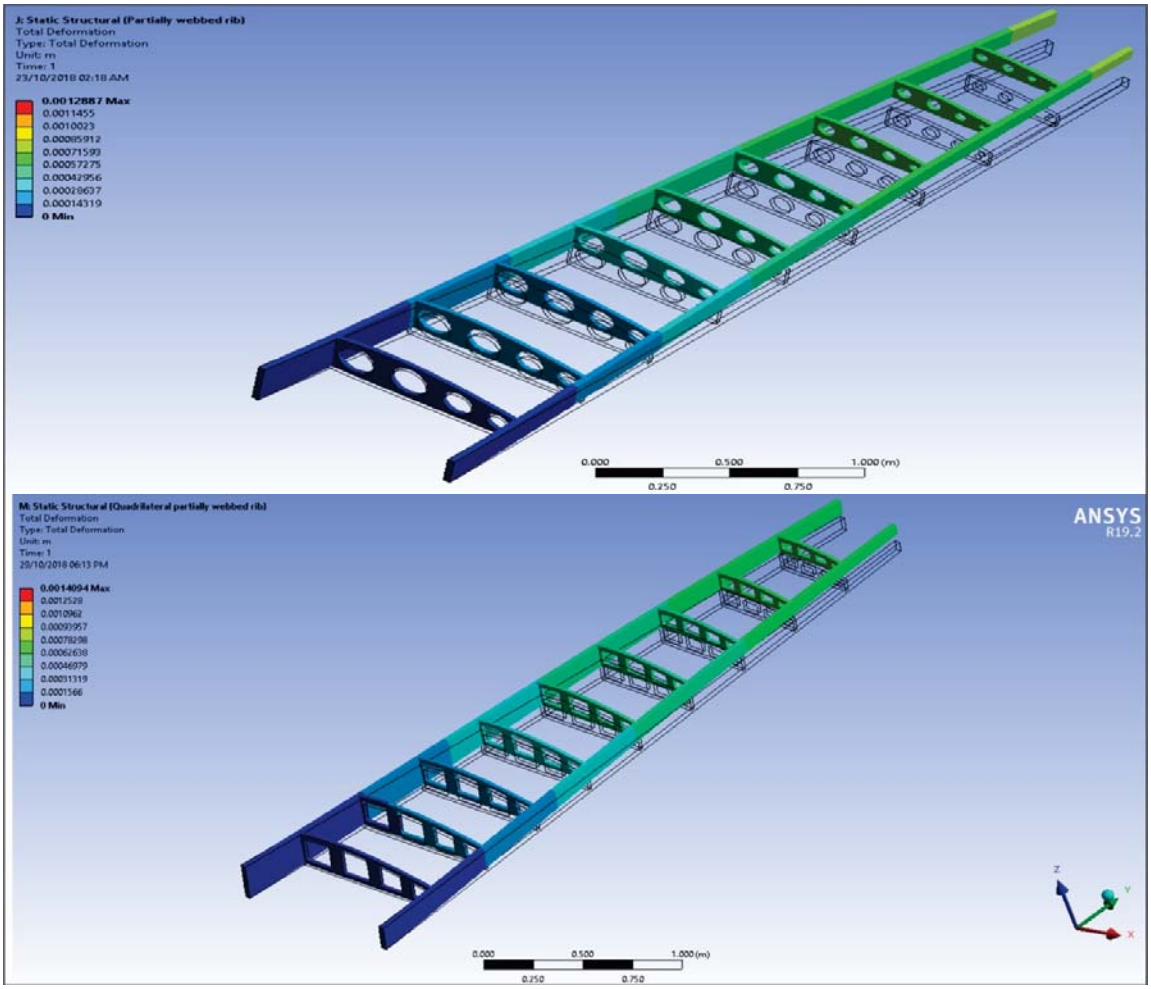

Figure 31 Total Deformation case2

As to be accepted, mush calculation is not done for total deformation since it is derivative of the equivalent stress. Observing the result shows that the maximum total deformation has dropped from 1.4094mm (second condition) to 1.2887mm in the first condition, as shown in the above table. This is also considered when selecting the wing-box CAD geometry.

4.4.5.3 Torsional Deformation (Directional)

Rib Conditions	Minimum [m]	Maximum [m]	Average [m]	Mass [kg]
Circular webbed	-2.5876e-005	2.9871e-005	3.2508e-006	306.12
Quadrilateral webbed	-2.5219e-005	3.2464e-005	3.1876e-006	300.13

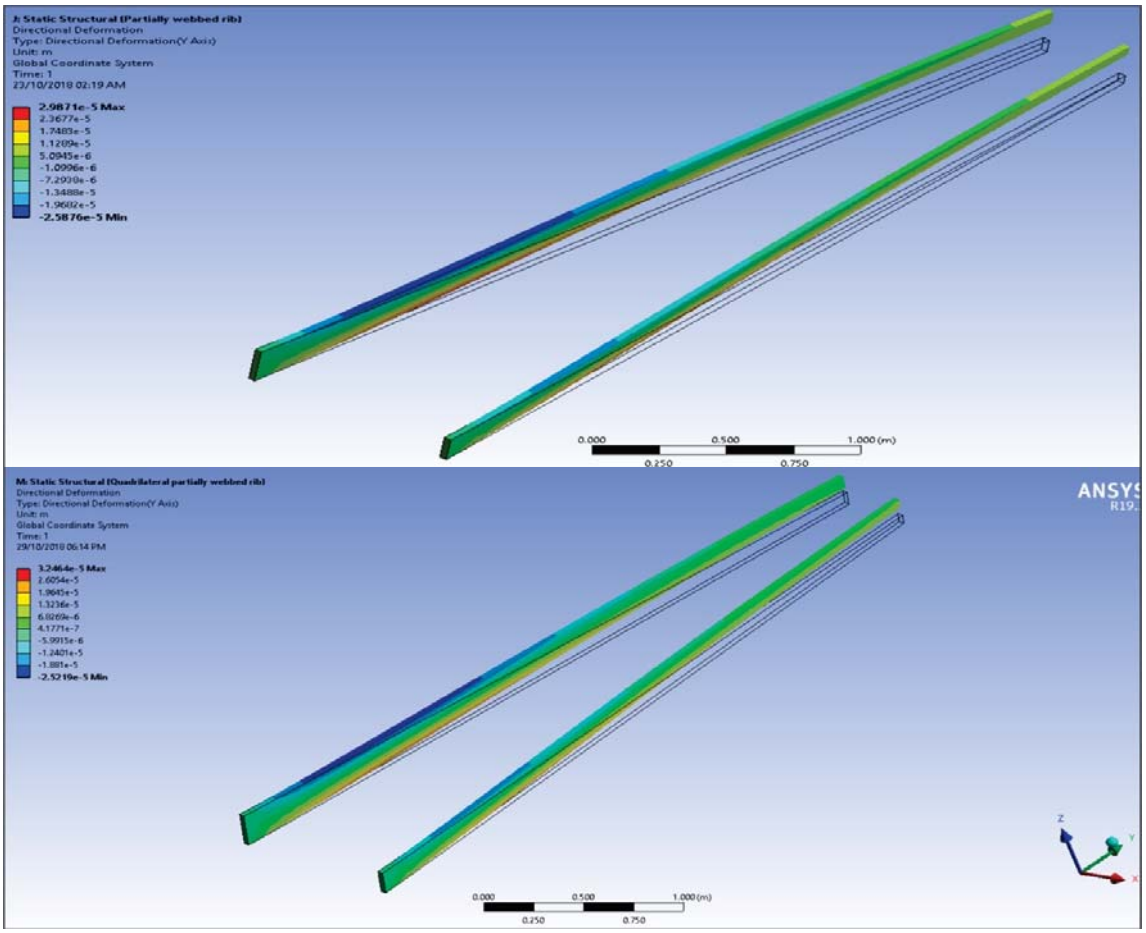

Figure 32 Torsional Deformation case2

The second condition seems to have slightly better average torsional resistance than the first condition which is significant is the wing-box CAD geometry selection, as shown above.

4.4.5.4 Result

Taking all the above criteria into consideration, it is obvious to see why the second condition (i.e. partially webbed rib of internal Quadrilateral boundary) has be chosen for further study and optimization. This condition has been analyzed in Ansys, and observed to have a better structure performance than the second condition

4.5 Conclusion

Considering all case studies, it is observed that the obtained results are very close to the suitable degree of structural tolerance for the wing-box at extreme condition of take-off loads. This can also be considered as a validatory study of the wing-box structural performance, which is valid for the selected wing-box CAD geometry for two-seater conventional aircraft. Hench the wing-box with partially webbed rib of internal Quadrilateral or Circular boundary are both very close performance. Hence both can be used for any future study.

5 PARAMETRIC OPTIMIZATION

5.1 Introduction

A series of optimization will be carried out using different parameter variations. These is done by comparing different iterative values of this components from;

- Varying the location of spar as; 15-20% chord length from the L.E. for the front spar. And 70-75% chord length from the L.E. for the rear spar. Note that we can't go beyond this range of values, because it will create structural difficulty for the proper allocation of fuel tank, ailerons and high lifting devices.
- Varying the thickness of the spars, ribs, stringers and skin surface

The objective of this analysis is to ensure that the important output parameter of mass, equivalent stress and minor output parameters such as total/torsional deformation are all in optimum value for the given amount variations. Therefore, all thickness variation must be within the expected mass limit of the wing structure to the aircrafts empty mass. This calculation will be considered in the optimization of thickness section.

N/B: Running these multiple thicknesses variational analysis will increase the complexity of arriving at an optimized value and also increase simulation time. Hence correlation for the thickness of all the listed above input parameter must be inertially considered. And also, it is important to note that the spar cross sections are not complex I section (i.e. they have no flange).

5.2 Optimization of Spar Positioning along Chord Line

After much days of repeated simulations with errors and re-modelling coupled with the fact that design point study for a Coupled Solution doesn't support RMS (remote machine solver).

Hence the following instructions and software must be used in order to ensure smooth simulation.

5.2.1 Software required

- CADNexus_CAPRI V3.21.0
- ANSYS 17.0
- Catia v5 R2015

5.2.2 Procedure

- The geometry is re-modelled with the selected conditions from previous analysis. This modelling is done in Catia v5 R2015, and the spars are made to be adjustable for the purpose of our simulation along the chord length, using suitable relational formulas. This directly proportional formula is created against an object which both spar share (e.g. the chord length between the spar). The two spar variation input parameters should contain _DS in their name for ease differentiation from the other parameters. Also publish name selection for the edges and surfaces as shown below, and save the model with. CATpart extension.

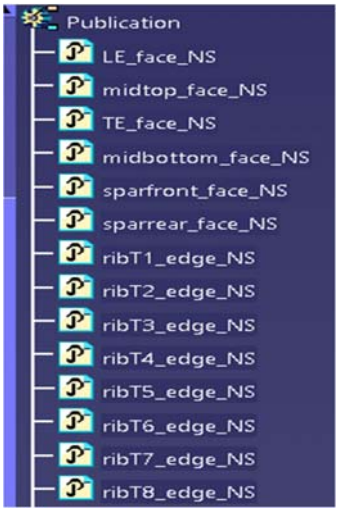

- Test the saved model for associative property through the CADNexus (CNExplorer), if the model loads properly then the model is ready for flawless parametric simulation.
- Open Ansys v17.0 and import the model, while ensuring the following setting are done in Ansys:
    - Set the periodic restart of Mechanical, meshing application to one design point, by clicking tools and then options menu.

- Suppress the fuel tank structural part.
- In the Geometry modeller set yes to using associatively, yes for parameters and set the parameter key as DS and yes to Name selection with no name selection key. And tick the spar parameters to publish them in the input parameter for the design point analysis.

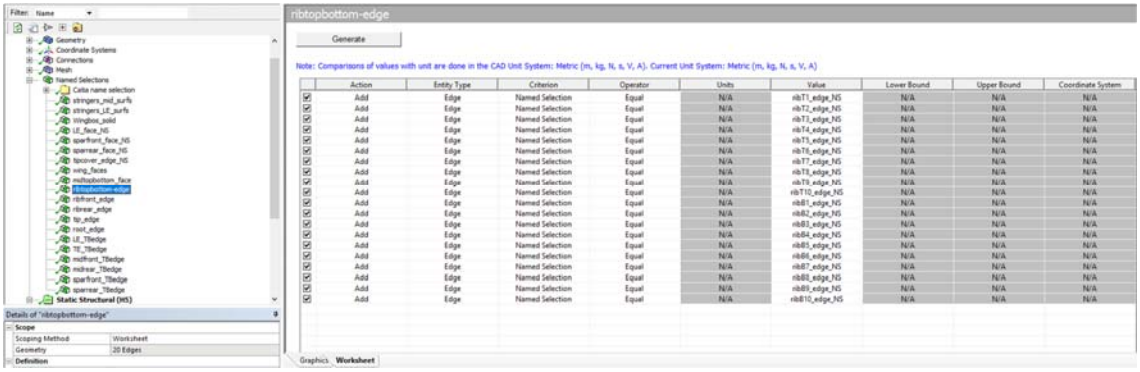

Figure 33 Name Selection worksheet for Ribs

- The meshing and setup are same as the previous analysis, but the number of iterations in the couple solution setup is reduced from five to three, because of simulation time for all design point and the output frequency is set to restart at every step interval. While in the model setup the name selection is done using the worksheet formula from the already created name selection (i.e. imported from Catia), to avoid errors during simulation. A pattern of this worksheet is shown below;

- The front spar location ratio from the LE in percentage is varied from 15-20%. And the Rear spar location ratio from the LE in percentage is varied from 70-75%. This will create a total of 11 design points.
- During design point update, it is important to run each update separately, to avoid unsolvable solution. By right clicking each design point and choosing to update the selected design point.

- Save the project, because it will be used for further analysis for the impact of the surface thickness to the wing box performance.

5.2.3 Parametric Result

Finally, we were able to obtain parametric values for both the front and rear spar positioning with respect to the leading edge (L.E). These data are represented in the tables below. It can be shown the implemented input (i.e. variation of spar location) and output parameters (i.e. equivalent stress, torsion and mass). The first table is for the Quadrilateral internal boundary rib and the second table is for the Circular internal boundary rib.

# The parameters defined in the project are:								
#	P1 - Front_Spar_Location.Ratio_DS	P2 - Rear.Spar.Location.Ratio_DS	P3 - Equivalent Stress Maximum [Pa]	P4 - Equivalent Stress Minimum [Pa]	Directional Deformation Maximum [m]	Directional Deformation Minimum [m]	P7 - Geometry Mass [kg]	Weight to equivalent stress ratio [m
#								
# The following header line defines the name of the columns by reference to the parameters.								
Name	P1	P2	P3	P4	P5	P6	P7	P8
DP 0	15	70	80.03E+06	47564.67	6.15E-04	-5.97E-04	268.99	3.36E-06
DP 1	16	70	72.92E+06	35360.86	6.15E-04	-5.87E-04	268.95	3.69E-06
DP 2	17	70	66.55E+06	49385.05	6.14E-04	-5.77E-04	268.83	4.04E-06
DP 3	18	70	76.21E+06	42767.76	6.14E-04	-5.69E-04	268.62	3.52E-06
DP 4	19	70	58.48E+06	37135.44	6.12E-04	-5.60E-04	268.33	4.59E-06
DP 5	20	70	62.18E+06	35660.63	6.10E-04	-5.52E-04	267.97	4.31E-06
DP 6	15	71	80.29E+06	67010.93	6.17E-04	-6.00E-04	269.11	3.35E-06
DP 7	15	72	81.03E+06	55317.94	6.21E-04	-6.05E-04	269.20	3.32E-06
DP 8	15	73	81.62E+06	60433.78	6.25E-04	-6.12E-04	269.25	3.30E-06
DP 9	15	74	82.33E+06	52837.61	6.30E-04	-6.18E-04	269.27	3.27E-06
DP 10	15	75	82.92E+06	40978.19	6.33E-04	-6.24E-04	269.25	3.25E-06

Table 3 Analysis data for Rib with Quadrilateral inner boundary for web

# The parameters defined in the project are:								
#	P1 - Front_Spar_Location.Ratio_DS	P2 - Rear.Spar.Location.Ratio_DS	P3 - Equivalent Stress Maximum [Pa]	P4 - Equivalent Stress Minimum [Pa]	Directional Deformation Maximum [m]	Directional Deformation Minimum [m]	P7 - Geometry Mass [kg]	Weight to equivalent stress ratio [m
#								
# The following header line defines the name of the columns by reference to the parameters.								
Name	P1	P2	P3	P4	P5	P6	P7	P8
DP 0	15	70	72.00E+06	59840.63	6.16E-04	-5.96E-04	274.17	3.81E-06
DP 1	16	70	71.00E+06	63962.01	6.16E-04	-5.88E-04	274.10	3.86E-06
DP 2	17	70	64.77E+06	47942.28	6.16E-04	-5.80E-04	273.95	4.23E-06
DP 3	18	70	74.22E+06	53997.90	6.14E-04	-5.68E-04	273.70	3.69E-06
DP 4	19	70	56.90E+06	9027.95	6.10E-04	-5.59E-04	273.36	4.80E-06
DP 5	20	70	60.41E+06	14610.72	6.09E-04	-5.52E-04	274.23	3.79E-06
DP 6	15	71	72.44E+06	76642.09	6.20E-04	-6.01E-04	274.19	3.70E-06
DP 7	15	72	72.92E+06	30222.93	6.23E-04	-6.06E-04	274.10	3.69E-06
DP 8	15	73	73.43E+06	21520.19	6.27E-04	-6.12E-04	274.25	3.76E-06
DP 9	15	74	74.01E+06	57573.98	6.31E-04	-6.18E-04	272.96	4.52E-06
DP 10	15	75	74.31E+06	11653.67	6.33E-04	-6.23E-04	274.23	3.73E-06

Table 4 Analysis data for Rib with Circular inner boundary web.

Comparing both results in the tables above we can say that the Circular inner boundary web is slightly better performing only in terms of mass to equivalent stress ratio. But from our previous studies when we had the fixed spar location, we saw the reverse case in terms of performance. Hence, we can state that Circular inner boundary web is more optimised for running analysis on variable spar location. Therefore, we will only be analysing the data in the second table in our future studies and observations.

From the above data we can see the important information be represented for each design point, while varying one spar location the other spar is kept constant at its base value. We understand that the lower the equivalent stress with respect to a fixed structural mass the better performing the design point. And we know that from the previous analysis that the equivalent stress is directly proportional to the total deformation, hence to avoid complication of the design table, which can also lead to insolvability of the solution. This is to say that the equivalent stress represents the ascertainable deformation, thus the total deformation information will be provided doing the finally simulation of the selected parametric geometry.

Before that, observing the table we can see that in varying front spar location, the maximum equivalent stress decreases from 15-17% and increases at 18% before decreasing again, and finally a slight increase at 20%. While the minimum equivalent stress increases from 15% and 16% before decreasing at 17% and then increasing again through to 20%. The torsional performance is observed to be slightly better as it varies from 15-20%.

That of the Rear spar location has a slight increase in maximum equivalent stress. And its minimum equivalent decreases up to 73% before increasing at 74% and then finally decreasing at 75%. And the torsional performance in this decrease slightly as it varies from 70-75%.

In order to properly interpret this data, it is important to view it from graphical representation, as shown below;

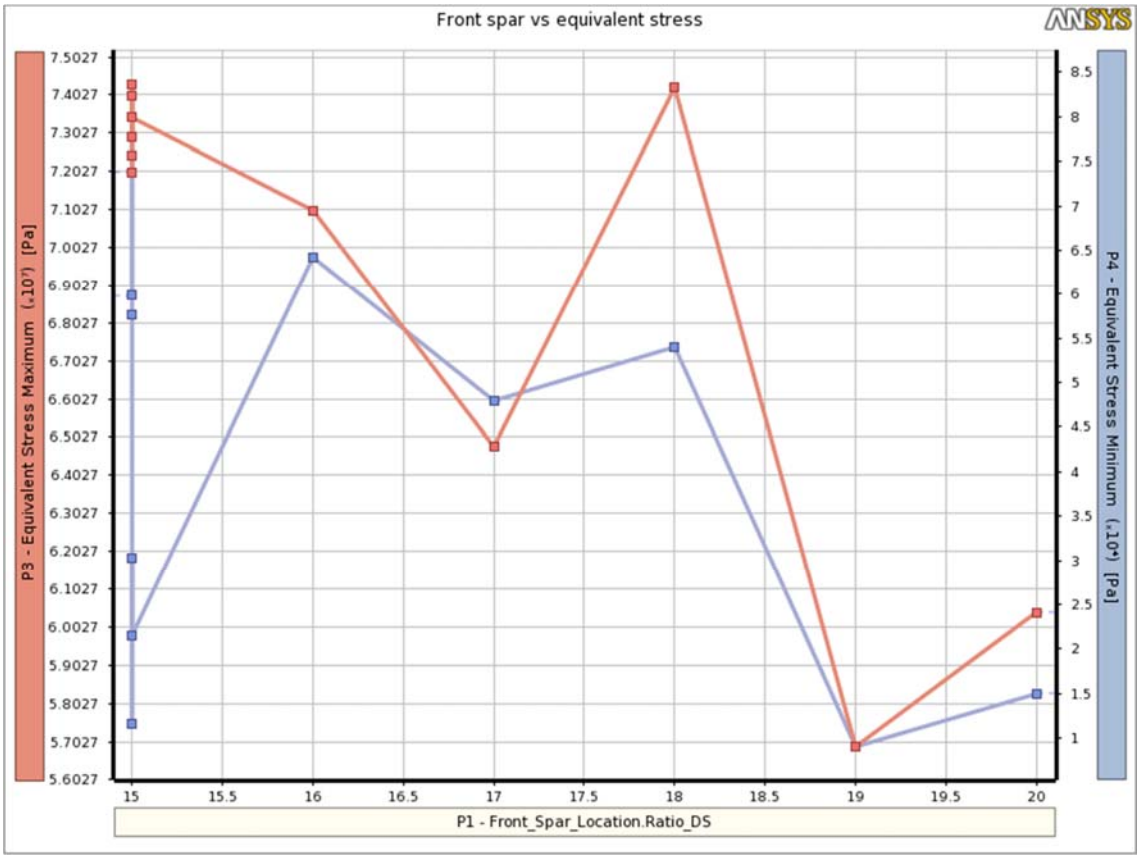

Figure 34 Front spar location vs Equivalent stress

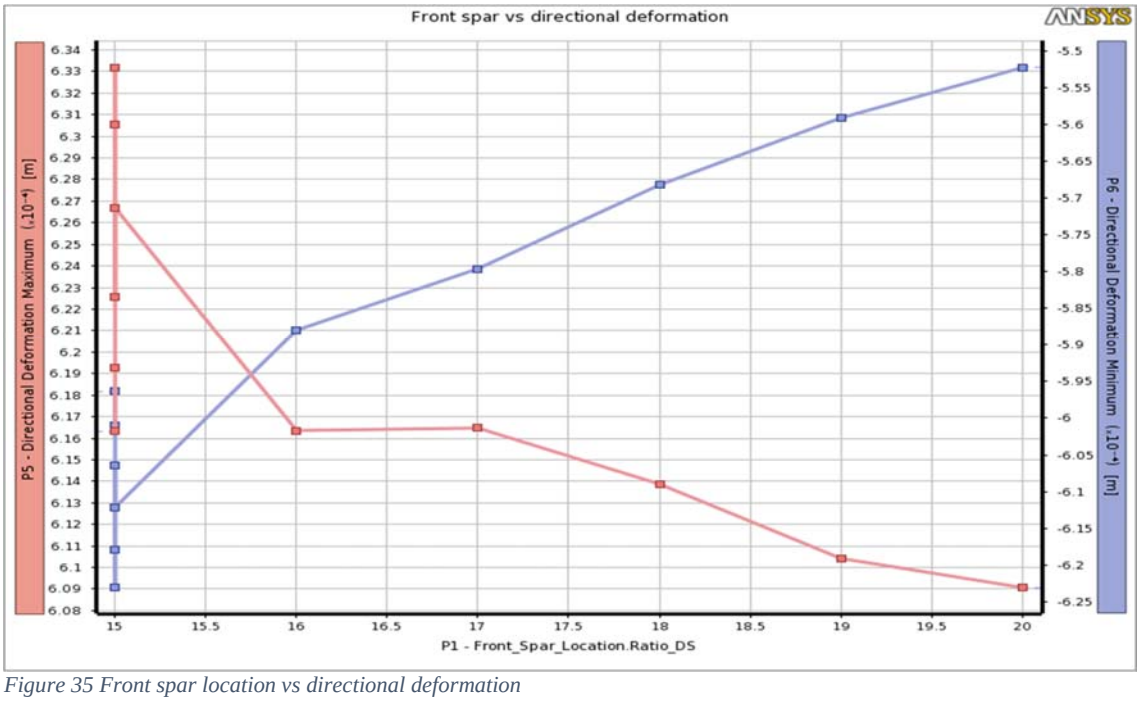

Figure 35 Front spar location vs directional deformation

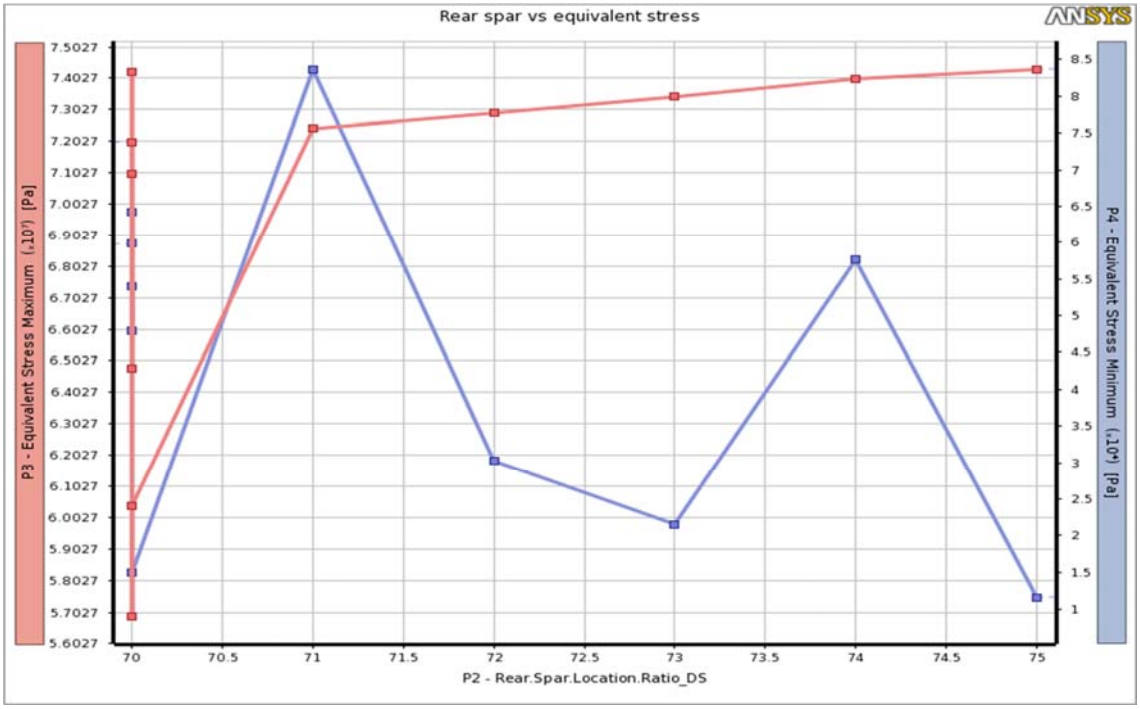

Figure 36 Rear spar location vs Equivalent stress

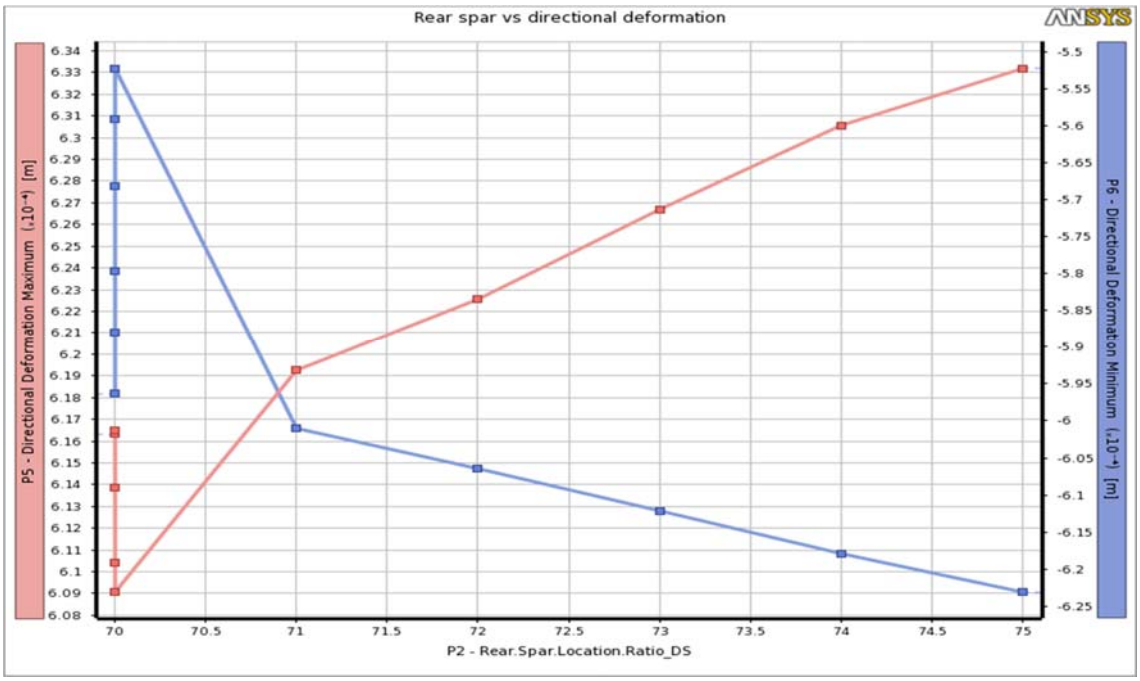

Figure 37 Rear spar location vs directional deformation

N\B that the red colour highlights the maximum data of a given graph, which is written on the left side.

5.2.4 Inference

We can insightfully say that from the varying the Front spar location we have two performing positions which are 19% and 20%, but 19% is slightly more performing both torsional and von-mises stress. And for the Rear spar location the 70% location seem to perform better both in torsional and maximum von-mises stress.

Now, to work with the mass optimization we have to consider the higher value for mass to equivalent stress ratio to be better performing or to simply understand this, we can assume that for the ratio of equivalent stress to mass, the better performing will be that having a lower value. Hence considering the reciprocal of this, will yield our idea of higher value means better performing for our ratio. The interpretation will be best understood with the graph provided below;

Figure 38 Mass to Equivalent stress ratio vs. Front Spar Position (Along the Root Chord Line)

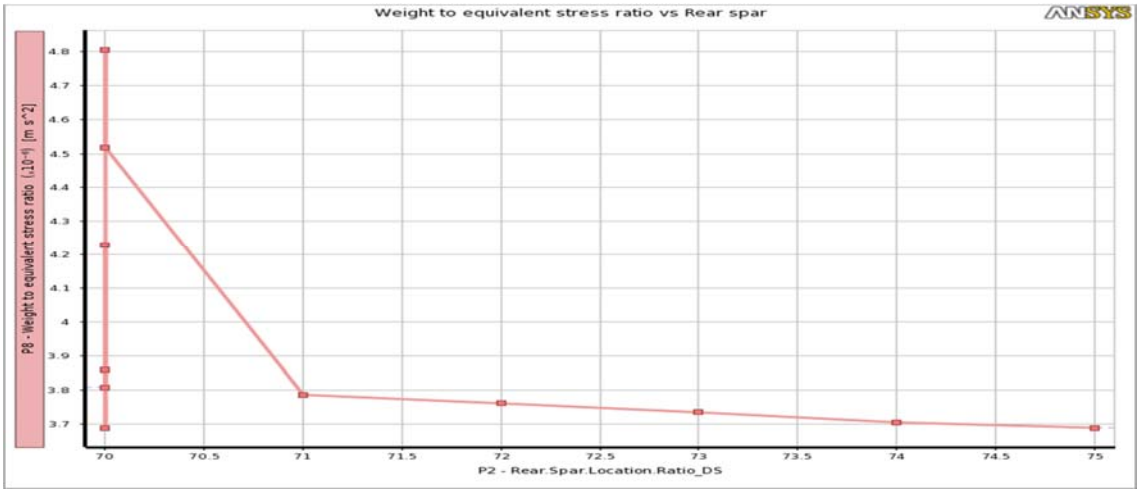

Figure 39 Mass to Equivalent stress ratio vs. Rear Spar Position (Along the Root Chord Line)

Hence the chosen values, which are analytically believed to be well optimized for the output parameters of mass, von-mises stress and torsional deformation are; location of the front spar at 19% from L.E along the chord line, and location of the rear spar at 70% from L.E along the chord line. We can conclude that the correlation of 19% and 70% of the Front and Rear spar location respectively has better performance than the correlation of 15% and 70% of the Front and Rear spar location respectively.

5.2.5 Conclusion

The mass to maximum equivalent stress ratio for quadrilateral inner boundary rib web (front spar at 15% of chord line and rear spar at 75% of chord line) and circular inner boundary rib web (front spar at 19% of chord line and rear spar at 70% of chord line) are 3.25e-6 and 4.80e-6

The improvement in performance for our selection of circular inner boundary rib web (front spar at 19% of chord line and rear spar at 70% of chord line) over the other is calculated below in percentage;

Percentage improvement in performance = ((4.80e-6 - 3.25e-6) / 3.25e-6) * 100% = 47.7%

Therefore, the optimization was indeed a success with an improvement in structural performance of 47.7%.

5.3 Optimization of Thickness Parameter

5.3.1 Introduction

To carry out this analysis we first have to update the selected spar location in the Catia software as shown below;

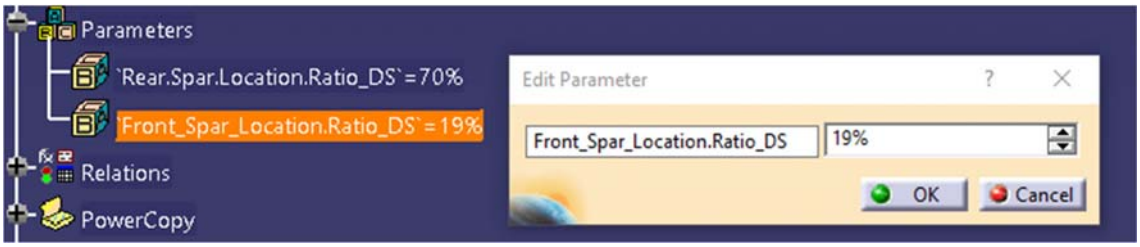

The model is then saved again for Ansys import in the design modeller tool. Only update function is perform and the required input parameters (i.e. Surface thickness) are ticked. Or by changing it in the Ansys Design-modeler parameter option of the imported CAD model.

Also, we know that thickness parameters of the spars, ribs, stringers, and skin surface will affect the overall mass of the wing proportionally. But common study suggest that the wing mass should be within 30-40% of the aircrafts empty mass. We consider that,

Wwing = 35% of Wempty

Wempty = 554.4kg (already obtained from the previous project study)

Therefore, Wwing for one wing = 194.04/2 = 97.02kg

Hence, the thickness input parameters should yield mass that is within the threshold of 97.02kg for the one wing box under analysis. To yield this mass the below values were inertially set;

- Spar thickness = 0.015m
- Rib thickness = 0.005m
- Stringers outer thickness = 0.0005m
- T.E. skin surface thickness = 0.001m (because of high expected deformation at this region compared to other skin surfaces)
- Other skin surface thickness = 0.0007m

This resulted to an inertial mass of 85.6kg and stress as shown in table below, which is exclusive of the fuel tank structural part.

Equivalent stress	Minimum [m]	Maximum [m]	Mass [kg]
Unoptimized thickness	30006	94.248e6	85.6

The mass to maximum equivalent stress ratio of this inertial Unoptimized thickness wing-box structure is calculated to be = 85.6 / 94.248e6 = 9.082e-7 kg/Pa

For organization purpose all ribs with same thickness are expressed to be equal to one rib thickness value, similarly with the spar, stringers and skin surface thickness (this done in the parameter set window of Ansys).

5.3.2 Correlational analysis of the thickness parameters

A polynomial relationship for the effectiveness of the input parameters to the output parameter is obtained. This analysis must be carried out first, in order to eliminate non-relevant parameter in the goal-based optimization.

5.3.2.1 Input Parameters

- Spar thickness varied from lower bound = 0.0135m to upper bound = 0.016m
- Rib thickness varied from lower bound = 0.0045m to upper bound = 0.0055m
- Stringers outer thickness varied from lower bound = 0.00045m to upper bound = 0.00055m
- T.E. Skin surface thickness varied from lower bound = 0.0009m to upper bound = 0.0011m
- Other-skin surface thickness varied from lower bound = 0.00063m to upper bound = 0.00077m

5.3.2.2 Output Parameters

- Equivalent stress, maximum and minimum.
- Total deformation, maximum and minimum.
- Torsional deformation, maximum and minimum.
- Geometry mass.

5.3.2.3 Correlation Convergence Setting

- Correlation type – Spearman (because we are dealing with interval scale and not ratio scale)
- Number of Samples – 50 (For a good result at a tolerable simulation period)
- Auto stop Type – Enable (This will skip a failed design point and move on to the next one)
- Mean Value Accuracy – 0.01 (The mean accuracy should be less than 1% from a previous step, for stable a correlation)
- Standard Deviation Accuracy – 0.02 (The deviation accuracy should be less than 2% from a previous step, for stable a correlation)

- Convergence Check Frequency – 10 (It checks if both the mean and deviation accuracy are stable for 10 design points, this makes a step)
- Filtering Method is kept at default for a relevance threshold of 0.5 (i.e. Parameter are considered as major input if their contribution is greater than or equal to 0.5), hence we set 5 maximum number of the major inputs (since we have an inertial five inputs, the simulation will filter out the minor output).

5.3.2.4 Correlation Matrix/Sensitivity Result

The correlation matrix and sensitivity charts are shown below:

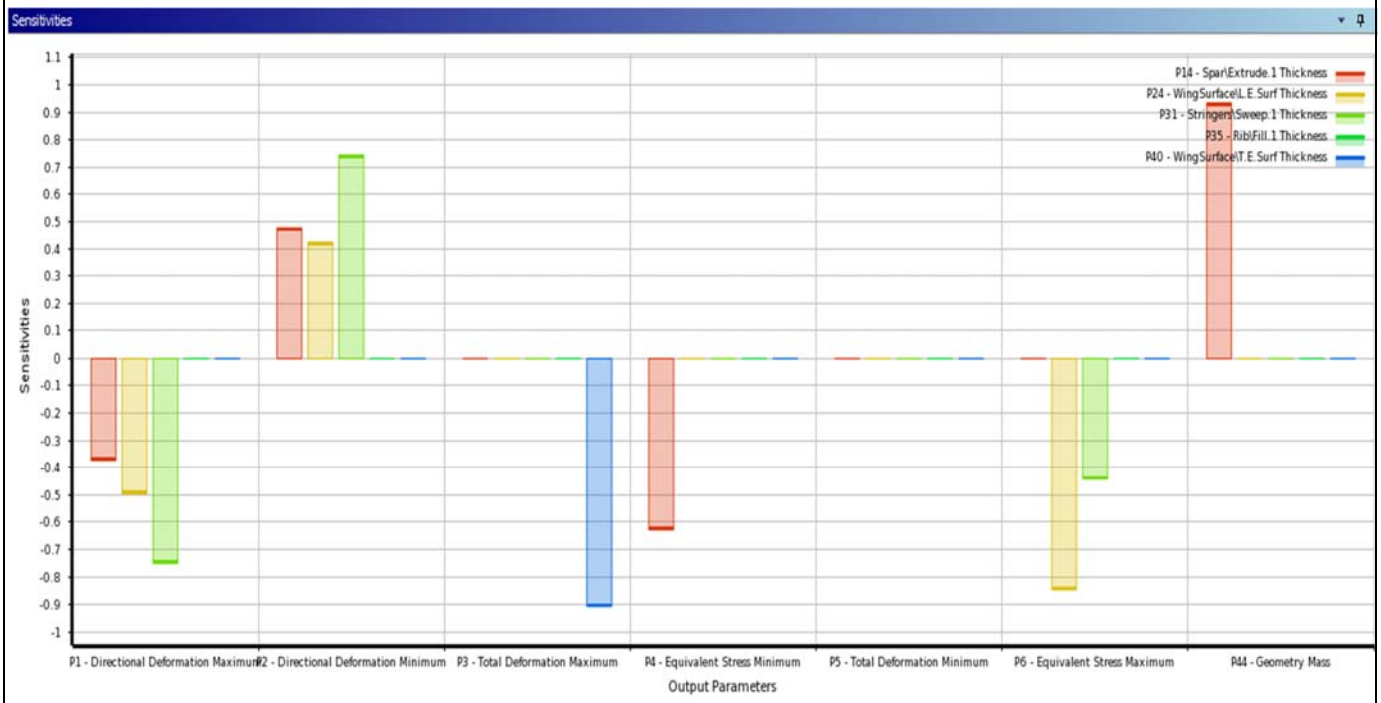

Figure 40 Output Sensitivity Chart

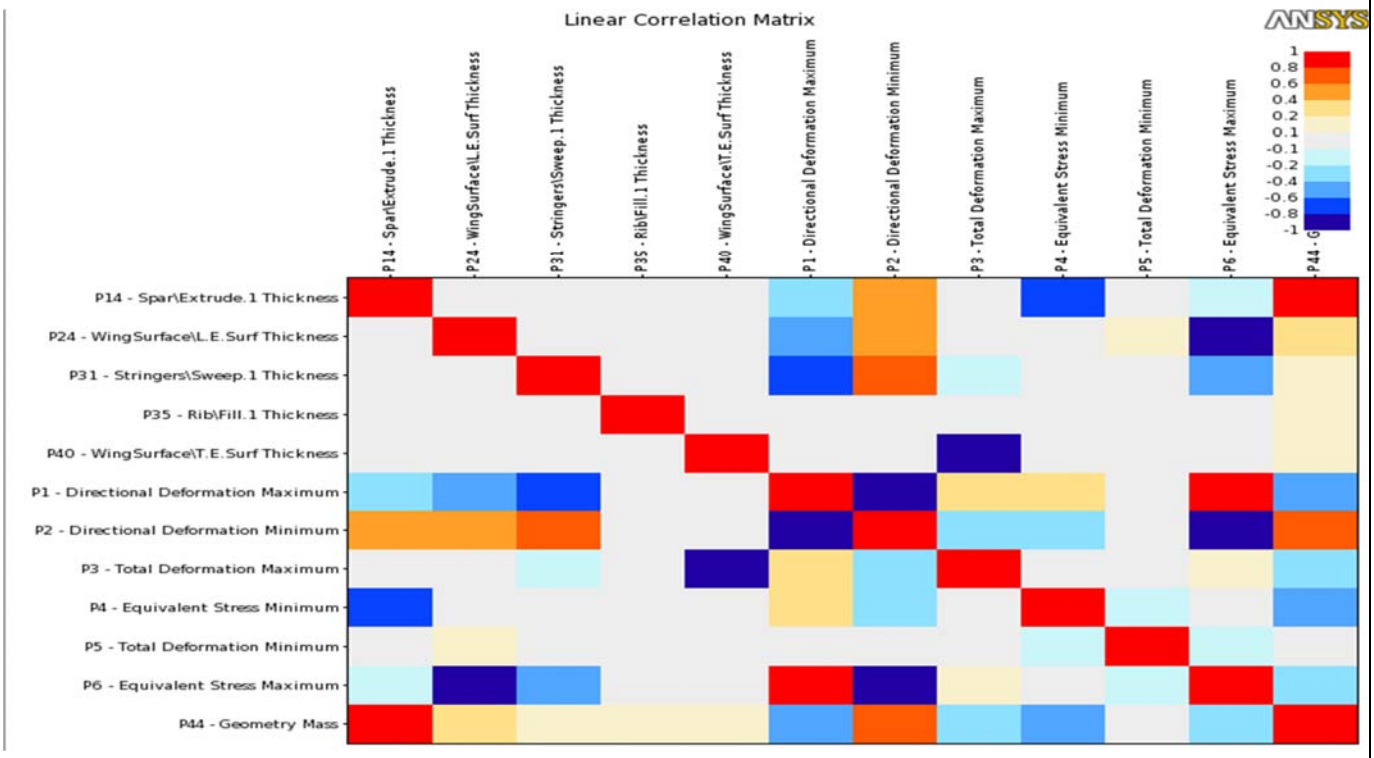

Figure 41 Input and Output Correlation Matrix

From the above the correlation matrix shows the relevance of any given input parameter to a given output parameter. This easily understandable through the visual color variation. The darker the color the more is its importance to a given output parameter. For example, observing the maximum equivalent stress parameter we can see that the other-skin surface thickness has higher relevance, followed by stringers and then the spar thickness. But the T.E. skin surface thickness and ribs seem to have very weak relevance to this particular output parameter.

Also, observing the sensitivity of maximum equivalent stress. We can see that this parameter is negatively sensitive to other-skin surface and stringers thickness. This means that increase any of these two input parameters will decrease the value of the output parameter.

For further information concerning this correlation study, other result chats such as determination histogram, determination matrix and correlation scatter (including its table and sampled design points), can all be observed to see the adaptiveness of this parameter to each other.

5.3.2.5 Inference

The schematic result of the input relevance to the filtered output below, gives us an idea of how negligible the effect of the ribs thickness parameter is to the output parameters under consideration.

Table of Schematic I2: Parameters Correlation

	A	B	C	D	E
1	Filtering Method				
2	Relevance Threshold	0.5			
3	Configuration	Filtering on Correlation Value and R2 Contribution, with a maximum of 5 major input parameters			
4	Filtering Output Parameters	P1 - Directional Deformation Maximum, P2 - Directional Deformation Minimum, P3 - Total Deformation Maximum, P4 - Equivalent Stress Minimum, P5 - Total Deformation Minimum, P6 - Equivalent Stress Maximum, P44 - Geometry Mass			
5	Major Input Parameters				
6	Input Parameter	Best Relationship With Filtering Output Parameter			
7		Relevance	Output Parameter	R2 Contribution	Correlation Value
8	P14 - Spar\Extrude.1 Thickness	1	P4 - Equivalent Stress Minimum	0.52464	-0.63211
9	P24 - WingSurface\L.E.Surf Thickness	1	P6 - Equivalent Stress Maximum	0.73696	-0.84169
10	P31 - Stringers\Sweep.1 Thickness	1	P1 - Directional Deformation Maximum	0.57352	-0.75176
11	P40 - WingSurface\T.E.Surf Thickness	1	P3 - Total Deformation Maximum	0.93289	-0.92053
12	Minor Input Parameters				
13	Input Parameter	Best Relationship With Filtering Output Parameter			
14		Relevance	Output Parameter	R2 Contribution	Correlation Value
15	P35 - Rib\Fill.1 Thickness	0.42695	P4 - Equivalent Stress Minimum	0.040831	0.16704

Table 5 of Schematic for Relevance of Input to Output

From the above table, we can observe that after the correlational simulation, that the ribs thickness parameter is filtered out as a minor input parameter with its low relevance and contribution to the output parameters. Hence yielding a very low correlation value.

Therefore, the ribs thickness parameter will be disabled for our future thickness optimization analysis under the design of experiment (DOE) menu. This will help reduce simulation time and also improve the goal optimization result.

5.3.3 Parametric optimization (goal-based optimization)

Response surface analysis will consider our output parameters as surfaces and will search through different design point to check the goodness of fit of the input to the output parameters.

5.3.3.1 Design of Experiment Setup

Set design of experiment type as Centre Composite Design. And design type as Auto Defined. This will generate 25 design points (DP) for the 4 enabled input parameters. We can increase the number of DP by changing design of experiment type as Custom + Sampling after the first 25 DP has been generated. And then set the total number of samples to be greater than 25. But this will increase simulation time, hence will sticked to 25 DP for this analysis.

The behavior of each DP to a given output parameter can be observed in the chart section of the DOE.

For the input parameters, we have to enable all parameter except rib thickness parameter. And use manufacturable values (or discrete values) of about 5 levels for each input parameter. These 5 level values must be within the range as listed below. Also, an example of spar thickness 5 level manufacturable values is shown below;

- Spar thickness varied from lower bound = 0.014m to upper bound = 0.018m
- Stringers outer thickness varied from lower bound = 0.0004m to upper bound = 0.0008m
- T.E. Skin surface thickness varied from lower bound = 0.0008m to upper bound = 0.0012m

Table of Outline A9: P40 - WingSurface\T.E.Surf Thickness

	A	B
1	Name	Manufacturable Values (m)
2	Level 1	0.0008
3	Level 2	0.0009
4	Level 3	0.001
5	Level 4	0.0011
6	Level 5	0.0012
*	New Level	

— Other-skin surface thickness varied from lower bound = 0.0006m to upper bound = 0.001m

5.3.3.2 Response Surface Result

The predictiveness of the DP frim its minimum and maximum search (learning points) for a given response surface is well described in the goodness of fit matrix or accuracy of results as shown below (disable to view the minimum of equivalent stress and total deformation response surfaces);

Table of Schematic J3: Response Surface

	A	B	C	D	E	F
1		P1 - Directional Deformation Maximum	P2 - Directional Deformation Minimum	P3 - Total Deformation Maximum	P6 - Equivalent Stress Maximum	P44 - Geometry Mass
2	Coefficient of Determination (Best Value = 1)					
3	Learning Points	0.99998	0.99999	1	1	1
4	Cross-Validation on Learning Points	0.99995	0.99997	0.99431	0.99999	1
5	Root Mean Square Error (Best Value = 0)					
6	Learning Points	1.0132E-07	7.5655E-08	4.8073E-06	11873	1.8853E-14
7	Cross-Validation on Learning Points	1.7836E-07	1.3582E-07	0.00017343	24883	3.4459E-14
8	Relative Maximum Absolute Error (Best Value = 0%)					
9	Learning Points	0.72564	0.58659	0.46913	0.20954	0
10	Cross-Validation on Learning Points	1.7849	1.1447	24.304	0.62052	1.366E-12
11	Relative Average Absolute Error (Best Value = 0%)					
12	Learning Points	0.30868	0.25086	0.15797	0.081573	0
13	Cross-Validation on Learning Points	0.53026	0.45201	4.043	0.16348	5.5735E-13

Table 6 of Schematic for Response Surface Goodness of Fit

We can see from the above that the DP has good predictive quality for any given response surface. Three stars indicate a high predictive quality, which means that Ansys can predictively generate appropriate input parameter for a given goal of response surfaces, with very low margin of error. This is very important for the goal-based optimization.

We can also observe the response of these surfaces by manually (local) inputting thickness value in the response point section, this will generate local sensitivity (with curve) and spider for that given inputted value. For example, we inputted:

- Spar thickness = 0.014m
- Other-skin surface thickness = 0.0006m
- Stringer outer thickness = 0.0004m
- T.E. skin surface thickness = 0.0008m

The local sensitivity is shown below (disable to view the minimum of equivalent stress and total deformation response surfaces);

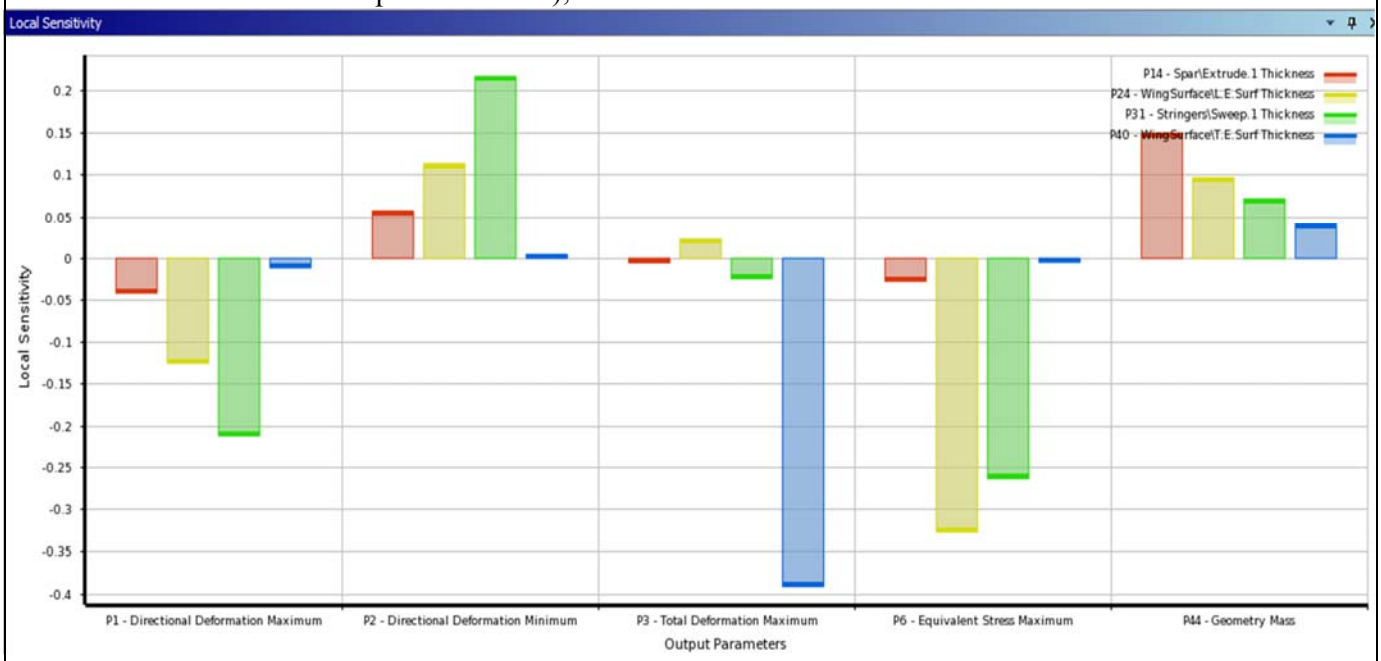

Figure 42 Response Surface Local Sensitivity

From the above chart we can easily interpret the individual effect of the input parameter to the enabled surfaces. For example, we can observe that T.E. skin surface thickness has very high effect on total deformation, whereas in other enabled response surfaces it seems to have very little effect on them.

5.3.3.3 Goal-Based Optimization

By specifying our goal, such as minimize the geometric mass, equivalent stress and total deformation. This will carry n number of permutations through a number of samples (1000 samples in our case), and will yield a number of optimized candidate (a maximum of 3 candidates in our case). Amongst these candidates one has to be selected which fits our goal and we perceive to be more suitable for the wing box structure. Below are the three candidates obtained:

Candidate Points

	Candidate Point 1	Candidate Point 1 (verified)	Candidate Point 2	Candidate Point 3
P14 - Spar\Extrude.1 Thickness (m)	0.014		0.015	0.016
P24 - WingSurface\L.E.Surf Thickness (m)	0.001		0.001	0.001
P31 - Stringers\Sweep.1 Thickness (m)	0.0008		0.0008	0.0008
P40 - WingSurface\T.E.Surf Thickness (m)	0.0012		0.0012	0.0012
P3 - Total Deformation Maximum (m)	0.0092913	0.0089519	0.0092057	0.0091173
P6 - Equivalent Stress Maximum (Pa)	6.3103E+07	6.3589E+07	6.2614E+07	6.214E+07
P44 - Geometry Mass (kg)	94.267	94.267	97.397	100.53

Table 7 of Schematic for Goal based Optimization Candidate Results

From the above table, we can observe that out of the three-candidate point, the candidate points 1 fulfills all our goal without any failure, unlike the other two candidate point which fail at geometry mass goal. Though candidate point 1 didn't yield any star for geometry mass goal, but it is a workable value. Hence, we select this candidate and right click on it to verify it through a full DP analysis (i.e. this will run the coupled simulation to verify the selected candidate).

After verification analysis we can observe a slight change in the goal result which is still workable and better than other candidate points. `We can view the different result charts like tradeoff (between two output surface), samples and sensitivities, in the result section for more understanding of the obtained and selected candidate point.

5.3.4 Conclusion

The mass to maximum equivalent stress ratio of this optimized thickness wing-box structure is calculated to be = 94.267 / 63.589e6 = 14.824e-7 kg/Pa

While, the mass to maximum equivalent stress ratio of this inertial unoptimized thickness wing-box structure has been calculated to be = 9.082e-7 kg/Pa

So that, the improvement in performance for optimized thickness over the inertial unoptimized thickness wing-box structure is calculated below in percentage;

Percentage improvement in performance = ((14.824e-7 - 9.082e-7) / 9.082e-7) * 100% = 63.2%

Therefore, this optimization is also a success with an improvement in structural performance of 63.2%.

5.4 Conclusion of Parametric Optimization

Deduction from this optimization analysis, presents the following optimized parameters:

- Ribs inner web boundary is set to circular geometry instead of the quadrilateral one.
- Front and rear spar position is set to 19% and 70% of chord line respectively from the L.E.
- Spars thickness = 0.014m
- T.E. skin surface thickness = 0.0012m
- Other-skins surface thickness = 0.001m
- Stringers outer thickness = 0.0008m
- Ribs thickness = 0.005m

The figure below shows the graphical implementation of this new optimized parameters in Ansys;

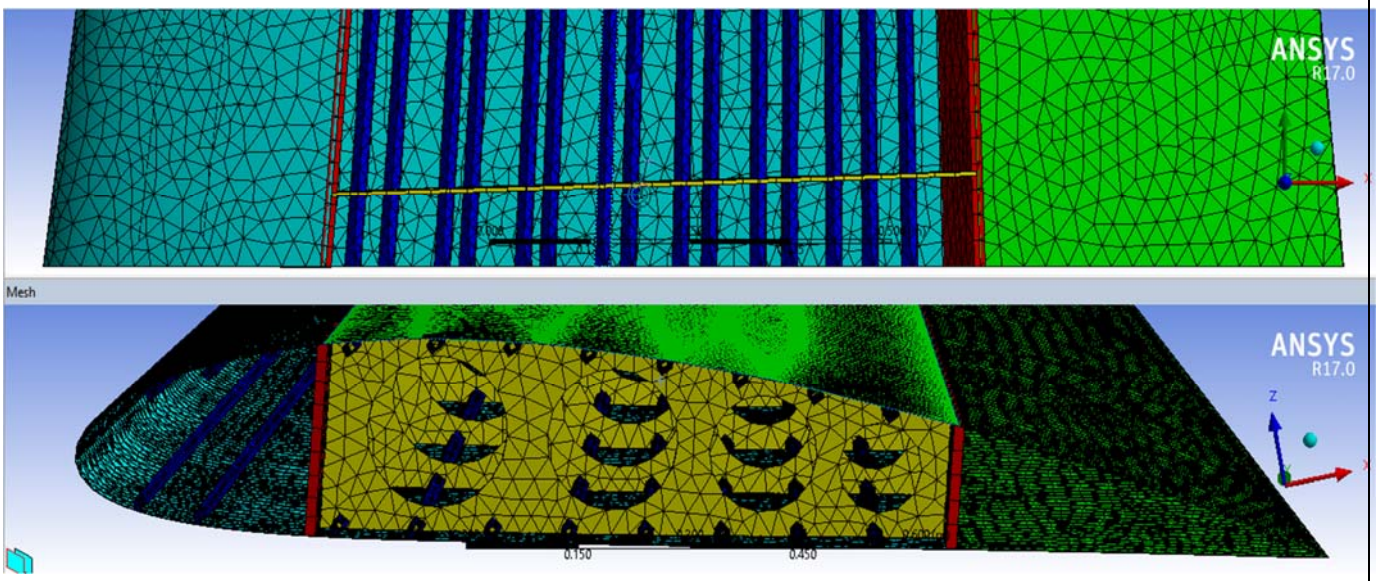

Figure 43 CAD Implemented Thickness Parameters

Implementing these verified optimized parameters into our wing-box structure will yield a sum performance improvement for spar location and thickness optimization. Which is calculated below as;

Total percentage improvement in performance = 47.7 + 63.2 = 110.9%.

What this means is that our wing-box structure mass to strength efficiency has been optimized by the following formula;

Optimized performance = (inertial performance) * 1.109 + (inertial performance).

Hence, we can conclude that the wing-box structural optimization was carried out through association of the CAD (using Catia software), and coupled CFD and FEA (in Ansys software).

6 WING-BOX FUEL TANK DESIGN EVALUATION

6.1 Introduction

To run a final structural analysis and validation we first need to un-suppress the fuel tank structure which is dimensioned as shown below;

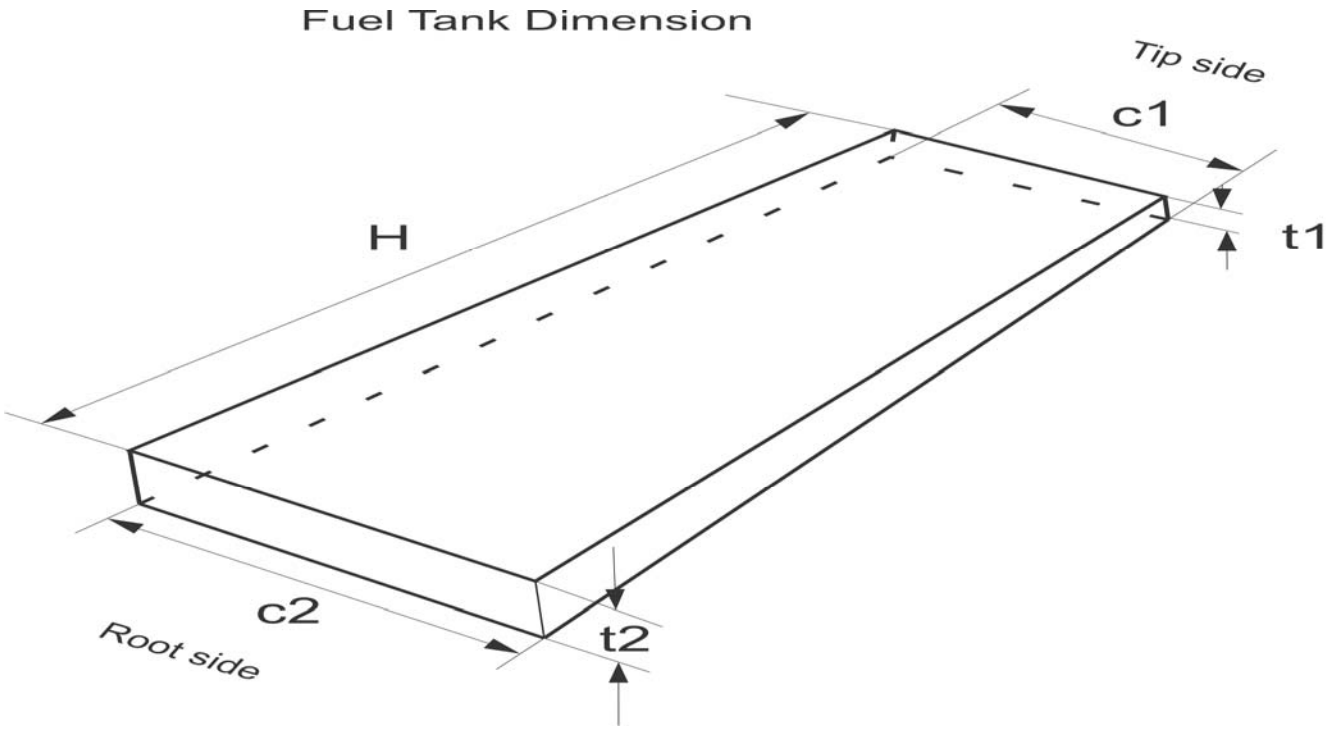

Figure 44 Fuel Tank Dimensional Parameter

6.2 Calculation of Fuel Tank Dimensional Parameters

The values for these dimensioned parameters are calculated below;

A = 0.9(0.5c)(t/c)(c) #please refer the previous project, on how these formulas were obtained.

V = H/3(A1+(√A1A2)+A2)

Mfuel = 0.70*785*V #we take volume lost due to structural interference as shown below to be 30%

Wfuel = 10*Mfuel

A1 = 0.9(t1*c1) = 0.9((0.15*0.1675)(0.5*0.670)) = 0.9(0.025125*0.335)

A1 = 0.007575m^2

A2 = 0.9(t2*c2) = 0.9((0.15*0.39415)(0.5*1.5767)) = 0.9(0.0591225*0.78835)

A2 = 0.04195m^2

But the actual model in Catia shows that A1 = 0.009m^2 and A2 = 0.048m^2. We will use these values to calculate the fuel tank volume;

V= 3.7/3(0.009+(√0.009*0.048)+0.048)

V = 0.096m^3

Mfuel = 0.70*785*0.096 = 52.75kg

Wfuel = 10*52.75 = 527.5N

This Wfuel is applied as force load onto the base of the fuel tank structure, in the static structure setup.

6.3 Wing-Box with Fuel Tank Evaluation Setup

Adding to the above, few setting and parameters are considered in the fluid flow (fluent) setup of the coupled system, but the procedures are same as before. These changes are described below:

We'll consider atmospheric turbulence of intensity = 0.16*Re^(-1/8)*100% with hydraulic diameter = 4A/P.

Calculated Reynolds number = 4687452

∴Turbulence intensity = 0.16*4687452^(-1/8)*100% = 2.34%

Cross sectional area of inlet, A = front_spar_area*cos15° + (0.81*Croot*sin15°)(one_wing_span)(vertical_taper_ratio).

A = 0.691*cos15° + (0.81*1.677*sin15°)(4.109)(0.4) = 1.245m^2

Wetted parameter of the wing = 10.006m^2

∴hydraulic diameter = 4*1.245/10.006 = 0.5m

These values are entered for the inlet/outlet boundary condition of k-epsilon model (realizable standard wall function).

The solution is initialized and re-run to obtain the below pressure distribution, taking initial turbulent kinetic energy of 3.6738m^2/s^2 with dispassion rate of 33.0588m^2/s^3.

6.4 Wing-Box with Fuel Tank Evaluation Result

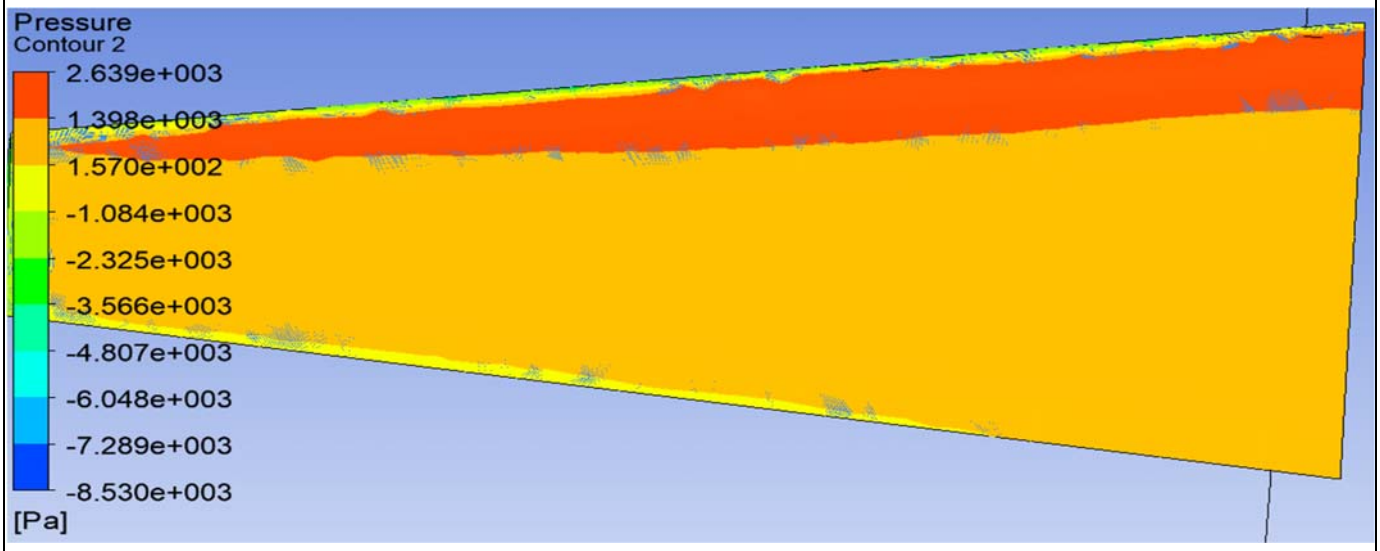

Figure 45 Pressure Distribution on the Bottom Wing Surface

This pressure values and its distribution (defined by the contour and colour, which are of significance at the bottom portion of the wing) will be used in future harmonic response analysis. The thickness of the aluminium sheet is set to 0.0005m, hence resulting to 100.51kg overall weight of this wing structure.

The FSI system is coupled and re-run with same settings. This yields the following results:

Solution Carried out	Minimum	Maximum
Equivalent stress (Pa)	28916	47.941e+006
Total Deformation (m)	0.	8.6009e-003
Directional Deformation (m)	-1.6166e-004	1.5443e-004
XY Shear Stress (Pa)	-1.0399e+007	2.1646e+007
YZ Shear Stress (Pa)	-7.7437e+006	2.472e+007
XZ Shear Stress (Pa)	-1.1149e+007	1.1012e+007

7 MODAL AND HARMONIC ANALYSIS

7.1 Introduction

Modal analysis is as important as carrying out a static structural analysis, because our aircraft will always experience exposure to different gust wind (which can cause turbulence) and vortex with different force frequency. If our structure is not properly design to with stand such frequencies (i.e. for the force frequency not to be equal to the natural frequency of our structure), it will lead to catastrophic failure of the structure. Natural frequency of structure will vary, depending on three key parameters. Which is the shape of the structure (stiffness/aeroelasticity), the material used in the structure and its damping ratio. We know that the higher the response of our structure to force frequency, the lower is its natural frequency, while damping ratio tend to increase.

Hence, we are going to run modal analysis on the selected wing box CAD model and check it harmonic response to different forced vibration frequency (which are within the gust and vortex force frequency for low attitude aircraft).

7.2 Modal Setup

The root edges are used for the fixed support as used in all previous analysis. Maximum modes to find is set to 6 (which is sufficient to cover six different fundamental frequency modes).

7.3 Modal Result

Table below shows the natural frequencies of the wing-box structure and its mode shape maximum total deformation from a minimum of zero;

Modes	Frequency [Hz]	Maximum Total Deformation [m]
1.	6.4758	1.9476
2.	8.1325	1.9

3.	9.58	1.8923
4.	11.37	1.9546
5.	12.834	1.9792
6.	14.484	1.8433

Mode shape figure for the six modes are shown below;

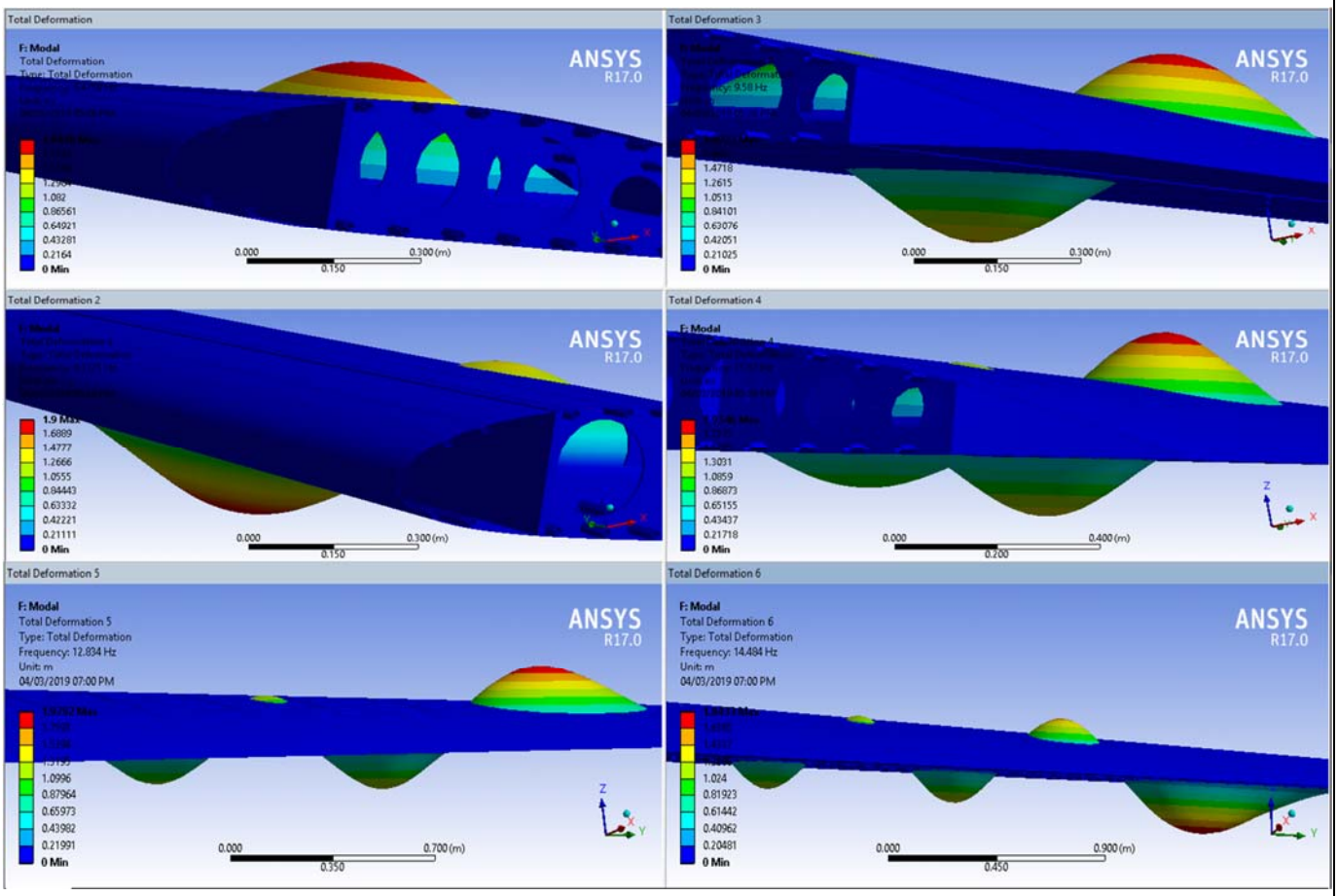

Figure 46 Six Modes of Wing-Box Natural Frequency Vibrational Deformation

As observed from the above figure, these low frequency modes seem to occur at the top surface of the fuel tank, which deform in the Z-axis for the entire mode. Hence to increase the natural frequency of the aircraft, a different fuel tank structure can be considered (e.g. the bag type), or increase the structural stiffness of the fuel tank to the wing-box structure. But note that the frequency shown above are within the safe band. Because from study carried out by Robert, John and Walter, on 'Airplane wing vibration due to atmospheric turbulence' as described in

the literature survey. From that, it is safe to assume that our structures lower natural frequency is well above the effects of the measured spectrum power of the gust and turbulence frequencies. Hence, we can continue with the Harmonic response of the wing-box structure.

7.4 Harmonic Response Setup

Frequency range is set from 0 - 15Hz (Since our natural frequency went up to 14.484Hz), with 15 solution intervals (This will display results for every change in 1Hz in linear form).
The root edges are used for the fixed support as used in all previous analysis. Wfuel is also applied as force load onto the base of the fuel tank structure. In order to apply and distribute the wind pressure force from figure 6.2, we have created a tabular data to apply a range of this force on the bottom portion of the L.E surface and the bottom portion of the remaining surface, separately, as shown below;

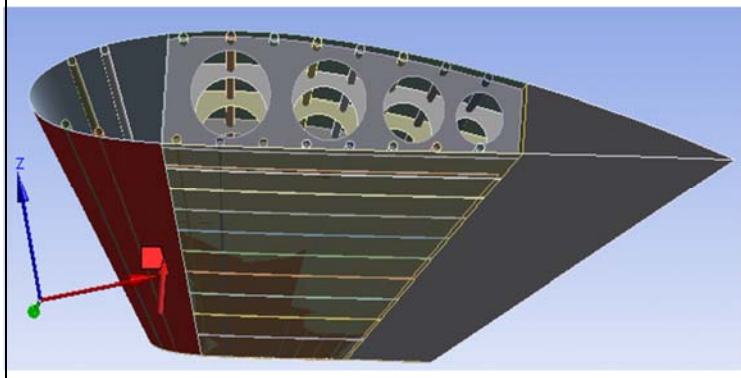

Tabular Data

	Frequency [Hz]	Magnitude [Pa]	Phase Angle [°]
1	0.	0.	0.
2	1.	1500.	0.
3	2.	1650.	0.
4	3.	1800.	0.
5	4.	1950.	0.
6	5.	2100.	0.
7	6.	2250.	0.
8	7.	2400.	0.
9	8.	2550.	0.
10	9.	2700.	0.
11	10.	2850.	0.
12	11.	3000.	0.

Figure 48 First Pressure distribution

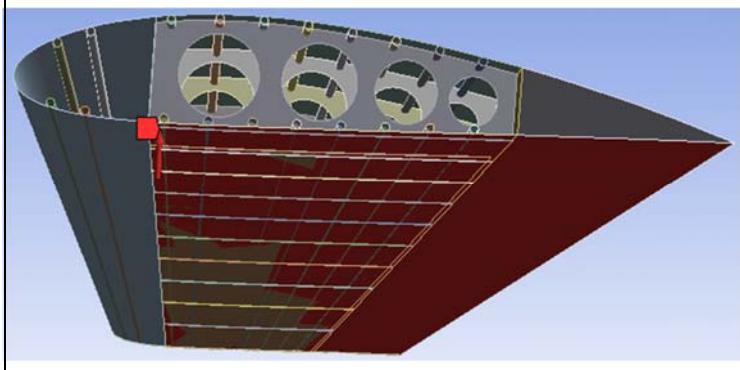

Tabular Data

	Frequency [Hz]	Magnitude [Pa]	Phase Angle [°]
1	0.	0.	= 0.
2	1.	250.	0.
3	2.	375.	0.
4	3.	500.	0.
5	4.	625.	0.
6	5.	750.	0.
7	6.	875.	0.
8	7.	1000.	0.
9	8.	1125.	0.
10	9.	1250.	0.
11	10.	1375.	0.
12	11.	1500.	0.

Figure 47 Second Pressure Distribution

7.5 Harmonic Response Result

Firstly, the we take a look at the frequency response graph, to study the change in amplitude of the vibration of the wing-box structure due to the applied load.

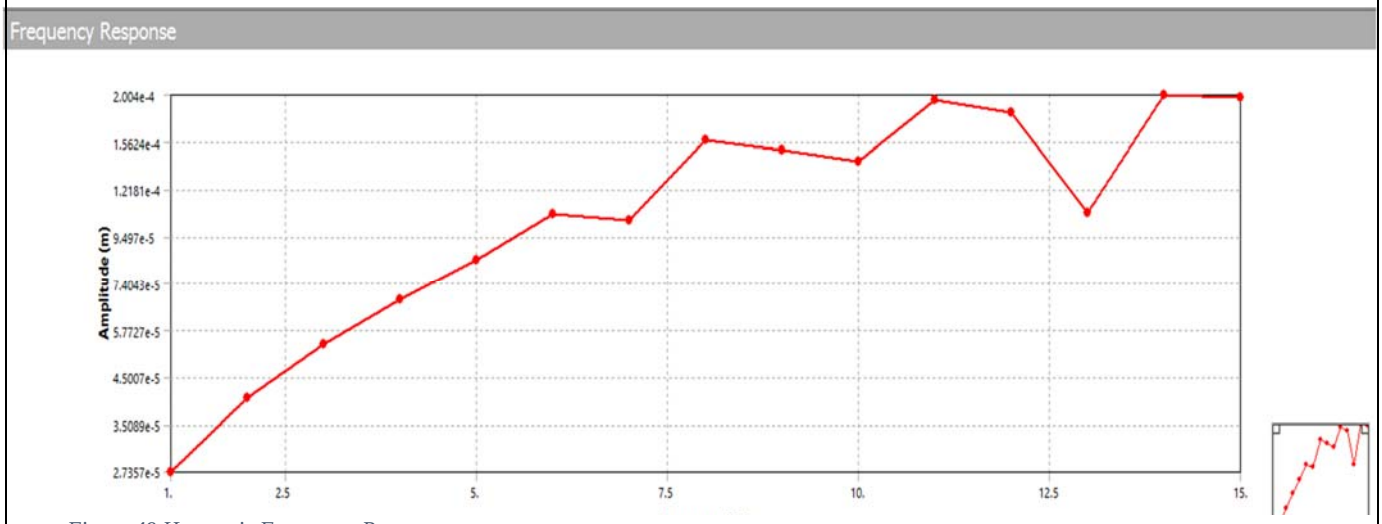

Figure 49 Harmonic Frequency Response

Frequency [Hz]	Amplitude[m]	Phase Angle[°]
1	2.7357e-005	0.
2	4.0322e-005	0.
3	5.375e-005	0.
4	6.7981e-005	0.
5	8.3845e-005	0.
6	1.0712e-004	0.
7	1.0381e-004	0.
8	1.5848e-004	0.
9	1.4979e-004	0.
10	1.4144e-004	0.
11	1.9565e-004	0.
12	1.833e-004	0.
13	1.0794e-004	0.
14	2.004e-004	0.
15	1.9717e-004	0.

The above reading is taken in the X-orientation (i.e. about the chord line orientation). The amplitude shows a steady increase up to the lower natural frequency (i.e. 6.4758Hz). And then decreases and increases again when the next gust and turbulence vibrating frequencies matches

the wing-box natural frequencies. And the amplitude decreases immediately after these frequencies.

We can view the impacts on the maximum total deformation of the wing-box when the gust and turbulence vibrating frequencies and the wing-box natural frequencies matches each other (i.e. Resonant frequency). This is tabulated and a graphical representation of it is done below;

Frequency [Hz]	Maximum Total Deformation [m]
6.4758	0.015537
8.1325	0.024167
9.58	0.023614
11.37	0.028391
12.834	0.050122
14.484	0.032724

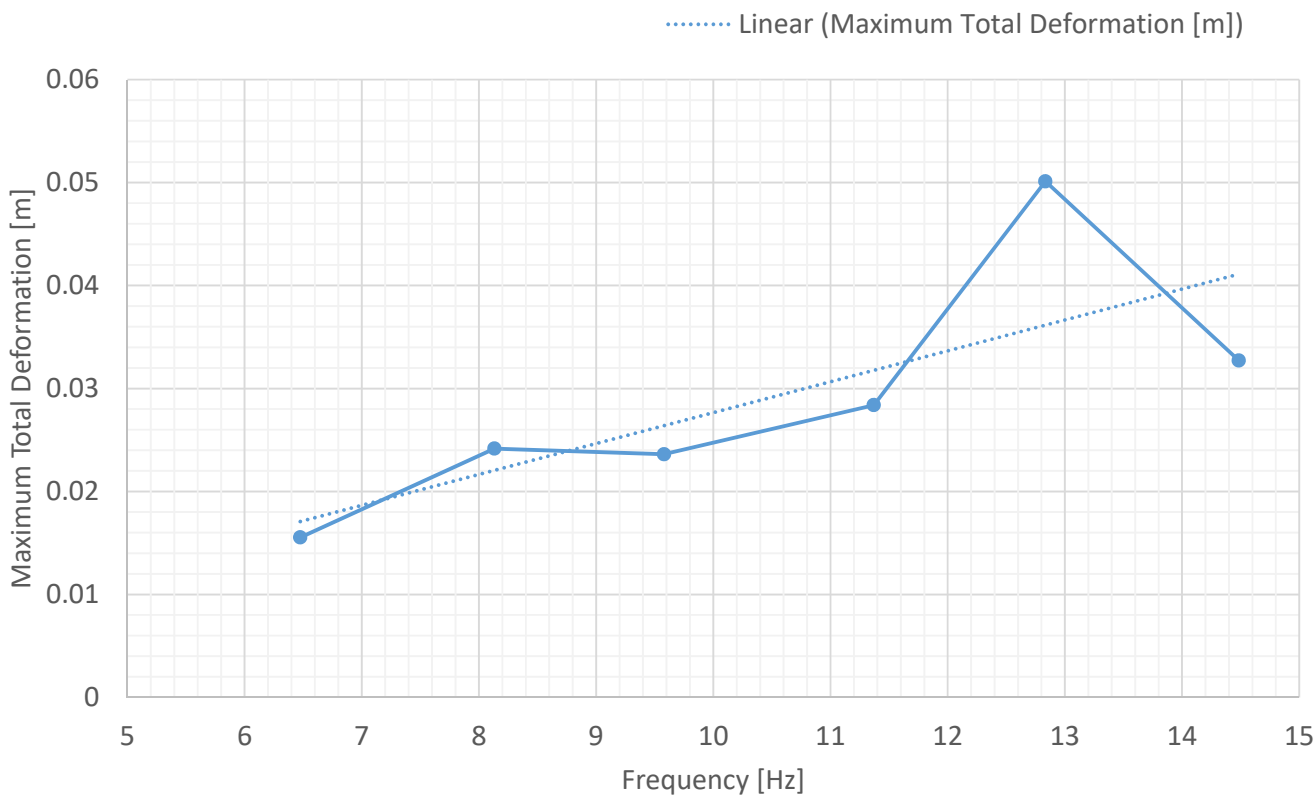

Figure 50 Frequency vs Maximum Total Deformation

Above graph shows the increase in total deformation as the resonant vibration frequency increases. And total maximum deformation experiences a peek value at 12.834Hz and at 8.1325Hz, which lies above the linearity line. It should be noted that there will be increase in the number of expected gust that the wing is to experience as altitude band increase or a reduction in the gust velocity.

N/B: For a more practical approach and result, the Prodera and HBM tools can be used which allows the use of visual sensors for both generating vibration and reading the modal response (through the strain gauges).

8 CONCLUSION

Computational design and analysis were carried out on a wing-box structure to evaluate its strength and resistance to resonant. Optimization was first carried out to improve its structural efficiency by 63.2% from its initial designed performance. Finally, a critical modal and harmonic response analysis was carried out to ensure that the wing box is capable of withstanding wind (turbulence/gust) vibration (i.e. its natural frequency is well out of range of the forced vibration frequency values). Hence the computational analysis was done with a high margin of success.

8.1 Scope for Future Work

We can proudly state that optimization of any given design/object is nearly infinite, because;

- Material property can be optimized, for its young's modulus, composites, structure etc.
- The shape of the object can also be modified in different ways. Like for our wing box structure, we can:

- Use different cross section (shape) for the stringers can be used also for parametric observation. Or even changing the diameter of this circular cross section.
- Vary the number of ribs and its location.
- Study different joint system, sizes, numbers etc (this could be rivetted, wedded, bolted etc)

9 REFERENCES

1. [1] Ambri; Ramandeep Kaur. “Spars and Stringers- Function and Designing”. Wing-box structure introduction.
2. [2] “Airframe Structural Design by Michael Niu” Airframe Structures. Published 1989.
3. [3] T. H. G. Megson. “Aircraft Structures for engineering students". Published 2012
4. [4] Immanuvel D.; Arulselvan K.; Maniiarasan P.; Senthilkumar S. (2013). “Stress Analysis and Weight Optimization of a Wing Box Structure Subjected to Flight Loads”. Weight optimization.
5. [5] Zhengran Yang; Yi Jiang; Cong Huang (2014). “The Thickness of an Aircraft Wing Skins Optimization Based on Abaqus”. Thickness Optimization.
6. [6] Robert L. Pastel; John E. Caruthers; Walter Frost (1981) “Airplane wing vibration due to atmospheric turbulence”. Aircraft vibrating spectrum.
7. “Conceptual Design of a Two Seat General Aviation Aircraft”. Conventional aircraft design. Istanbul university.
8. By John B.; Wheatley (1931). “Torsion in wing box” Torsional formulation on wing.
9. Eduhive (2018). “Design and Structural Validation of Aircraft Wing”. Aircraft design CAD.
10. Lica Flore; Albert Arnau Cubillo, (2015) “Dynamic Mechanical Analysis of an Aircraft Wing with Emphasis on Vibration Modes Change with Loading”. Modal Analysis.
11. N. I. Bullen (1957). “The Variation of Gust Frequency with Gust Velocity and Altitude”. Gust Frequency.
12. Prof. E.G. Tulapurkara “Airplane design (Aerodynamic)”. Aircraft Weight Contribution.
13. “U.S. Standard Atmosphere Air Properties SI Units”. Air Property. https://www.engineeringtoolbox.com/standard-atmosphere-d_604.html. Retrieved 2018-09-05
14. Air-foil Coordinates. http://m-selig.ae.illinois.edu/ads/coord/naca4412.dat. Retrieved 2018-08-24
15. Air-foil Lift Coefficient. https://my.solidworks.com/reader/forumthreads/91471/lift-coefficient-on-2d-airfoil. Retrieved 2018-08-25
16. Wing CAD Modelling in Catia. https://wsww.youtube.com/watch?v=LAIB7qK-9pE&t=877s ; https://www.youtube.com/watch?v=BFnkZGx218s. Retrieved 2018-08-29

LIST OF SYMBOLS AND ABBREVIATIONS

Cp	Coefficient of pressure
Cl	Coefficient of lift
Cd	Coefficient of drag
Cm	Coefficient of moment
m	meters
kg	Kilogram
N	Newton
μ	Dynamic viscosity
ρ	Density
P	Pressure
v	Velocity
a	Speed of sound
M	Mach number
T	Temperature
R	Universal gas constant
α	Angle of attack
δ	Boundary layer thickness
K	Kelvin
u	Freestream velocity
NACA	National Advisory Committee for Aeronautics
Croot	Root Chord
Ctip	Tip Chord
L.E.	Leading Edge
T.E	Trailing Edge
bwing	Wing Span
Λ	Sweep angle